Q. J. R. Meteorol. Soc. (1990), **116**, pp. 337–362 551.515.21

A numerical study of tropical cyclone motion using a barotropic model. I: The role of vortex asymmetries

By ROGER K. SMITH and WOLFGANG ULRICH

Meteorologisches Institut, Universität München, Theresienstr. 37, 8000 *München* 2, *Federal Republic of Germany*

and

GARY DIETACHMAYER[1]

Department of Mathematics, Monash University, Clayton, Australia, 3168

(Received 28 February 1989; revised 6 September 1989)

SUMMARY

The motion of an initially symmetric vortex on a beta plane and the motion of initially asymmetric vortices on *f* and beta planes are studied using a nondivergent, barotropic model. It is assumed that there is no basic flow, the effects of a basic flow will be addressed in part II. Parameter values such as vortex size and strength and computational domain size are chosen for their relevance to tropical cyclones. The simultaneous evolution of the asymmetric vorticity and streamfunction fields is investigated in terms of a partitioning of the flow introduced by Kasahara and Platzman in which all asymmetries are regarded as part of the vortex environment. It is shown that in this partitioning the asymmetric streamflow provides a 'steering current' for the vortex to a very close approximation.

For early times, typically 24 h for the parameters chosen, the development of the asymmetries in the vortices studied can be largely understood in terms of a simple analytical theory in which the vortex centre is fixed and the initial absolute vorticity distribution is rearranged by advection by the (initial) symmetric circulation. The shearing effect of this mechanism alone would appear to preclude the establishment of a true steady state in the flows considered.

The numerical calculation for the initially symmetric vortex on a beta plane is used to assess averaging procedures for computing the environmental wind field of a tropical cyclone from observed wind data. The results show that the averaging regions that have been commonly employed in observational studies are too large to properly characterize the environmental flow at the cyclone centre and they suggest caution in making inferences from these studies in relation to physical mechanisms such as beta drift.

The calculations for initially asymmetric vortices on an *f* plane show that the effects of the asymmetry on motion depend strongly on the scale of the asymmetry compared with that of the vortex. When the scale of the asymmetry is relatively small, the asymmetry is rapidly degraded by tangential shear and its effect on motion is not sustained. In contrast, larger asymmetries have a more persistent effect on motion. When the motion takes place on a beta plane, asymmetries induced by the advection of planetary vorticity ultimately dominate those present initially and, irrespective of the scale of the initial asymmetry, the vortex track finally turns to the north-west as in the case of the initially symmetric vortex. Finally, as a case of extreme asymmetry we study the mutual interaction of a strong vortex and a weak one. The behaviour is similar to that just described, the weak vortex merging with the stronger one. The analytical theory also proves useful in understanding the evolution of initial vortex asymmetries.

The interpretations of the calculations add insight into the dynamics of tropical cyclone motion, complementing the findings of recent studies by Chan and Williams and Fiorino and Elsberry.

1. INTRODUCTION

Early theories of tropical cyclone motion considered the motion of an initially symmetric vortex in a barotropic flow and sought to predict the short term displacement of the vortex centre (Sasaki and Miyakoda 1954; Sasaki 1955; Kasahara 1957). The prediction was based on an application of the barotropic vorticity equation at some hypothesized 'steering level' and the vortex centre was defined as the minimum in the vortex streamfunction. Sasaki (1955) and Kasahara (1957) showed that the vortex centre moved with a speed close to that of the steering current at that point, but with a drift at right angles to, and, in the northern hemisphere, to the left of the direction of the

[1] Present address: Bureau of Meteorology Research Centre, P.O Box 1289K, Melbourne, 3001, Australia.

absolute vorticity gradient of the steering current, the drift speed being proportional to the gradient (on account of this drift, of course, the term 'steering current' is a misnomer and we shall use the terms *basic current* or *environmental flow*, terms that will be precisely defined later). Thus an initially symmetric vortex on a beta plane with no basic current suffers a westward displacement of its centre in both hemispheres. Kasahara showed that this displacement was associated with the evolution of a wavenumber-one asymmetry in the vortex structure caused by the advection of planetary vorticity by the vortex, a result obtained independently by Adem (1956), but typical speeds were found to be small, no more than a few kilometres per day. In a subsequent paper, Kasahara (1960) extended his earlier analysis to a two-layer baroclinic vortex.

The foregoing theories are essentially diagnostic theories for the initial motion tendency in the same spirit as Sutcliffe's development theory for extratropical cyclones (Sutcliffe 1947); they do not consider the mutual interaction of the cyclone and the environmental flow. Such an interactive theory was developed by Kasahara and Platzman (1963). These authors discussed ways to partition the flow between the cyclone and its environment and they described a prognostic method for determining the cyclone motion, simultaneously with the evolution of the environmental flow. In their choice of partition, the cyclone was represented by a symmetric vortex that translates without change in structure, while the environment was defined as the residual flow. The equation for the latter was solved using a finite-difference method. In principle, the method is broadly equivalent to solving the barotropic vorticity equation directly, but by removing a vortex from the total flow, it was hoped that one would not need such a high resolution as would otherwise be the case. In practice the method is limited by the assumption that the 500 mb level (or any other level) serves as an approximate steering level, as well as by inaccuracies inherent in determining the appropriate initial fields over data-sparse oceanic regions, including the determination of the initial symmetric vortex. In addition to the vortex drift relative to the environmental flow discussed above, Kasahara and Platzman inferred a component of vortex *acceleration* in the direction of the absolute vorticity gradient of the steering current. In the case of an initially symmetric vortex at rest on a beta plane, this acceleration can be attributed to the advection of the vortex by an asymmetric 'secondary circulation' that is associated with the evolving wavenumber-one asymmetry in the vortex field referred to above (Anthes 1982). In Kasahara and Platzman's method of partitioning, referred to as method III in their paper, the secondary circulation is regarded as a part of the environmental flow.

In their efforts to develop a barotropic vortex model for operational tropical cyclone track prediction, Sanders and Burpee (1968) pointed out the inaccuracies of using radiosonde-derived pressure-height data in the tropics as used in earlier studies. Subsequently, Sanders and co-workers (Sanders 1970; Sanders *et al.* 1975, 1980) showed that improved skill in track forecasts could be achieved in general by applying the barotropic vorticity equation to a pressure-weighted vertical average of the tropospheric winds, in conjunction with an initial analysis based directly on the observed winds. These investigations concentrated mainly on the operational applications and especially on the problems of constructing an adequate initial analysis.

Studies which focused more on the dynamics of vortex motion were carried out by Anthes and Hoke (1975), Kitade (1980), Holland (1983) and DeMaria (1985). In particular, DeMaria solved the nondivergent barotropic vorticity equation using a spectral method and confirmed the importance of the absolute vorticity gradient of the imposed basic current on vortex motion. A notable result was his demonstration that the vortex track is sensitive to the initial position when the vortex lies in a region where the Laplacian of the absolute vorticity of the imposed basic current is positive.

The role of the planetary vorticity gradient on the vortex motion was examined in detail by Chan and Williams (1987; henceforth referred to as CW) and Fiorino and Elsberry (1989; henceforth referred to as FE), again in a nondivergent barotropic model. Both papers consider the motion of an initially symmetric vortex on a beta plane with no externally imposed flow. CW investigated the linear problem analytically and compared the results with numerical integrations of the nonlinear equations using a finite-difference method. They showed that the initial vortex projects onto Rossby wave modes that have a westward component of propagation. Accordingly, wave modes representing the outer circulation of the vortex have lower wavenumbers and travel faster than those representing the inner circulation. This leads to a stretching of the vortex towards the west. In the linear case, there is only a small westward displacement of the vortex centre, the latter being characterized by either the vorticity maximum or the streamfunction minimum. Significantly, however, the streamfunction minimum suffers a larger displacement than the vorticity maximum, implying a poleward component of the flow across the vortex centre. In the nonlinear case, this component is important and leads to a poleward component of vortex motion. These interpretations are consistent with those of earlier workers (e.g. Anthes 1982; Holland 1983) where prominence was given to the induced secondary circulation. CW's calculations showed that the vortex ultimately tracks north-westwards, accelerating at first and finally attaining a steady speed. For a fixed profile of tangential velocity, this speed is proportional to the relative circulation of the vortex core, $2\pi r_{\max} v_{\max}$, $v_{\max}$ being the maximum tangential wind speed and $r_{\max}$ the radius at which this occurs. However, FE have shown that for a fixed core circulation, the speed increases as the region of strong winds outside the radius of maximum wind extends radially outwards, although the speed is relatively insensitive to changes in the wind profile inside the radius of maximum wind.

FE discussed the nature of the interactions that bring about the steady north-westward translation. They calculated the contribution of the various terms in the streamfunction tendency equation and showed that in the quasi-steady state where the vortex tracks steadily north-westwards, the east–west asymmetry in the tendency associated with the linear beta effect is approximately balanced by the nonlinear term. In the latter, the dominant contribution is from the advection of the symmetric vorticity component by the asymmetric motion. In turn, this is opposed by the advection of the asymmetric vorticity by the symmetric circulation. Unfortunately, FE did not show the vorticity and vorticity tendency fields, although these must be regarded as fundamental (see e.g. the discussion by Hoskins *et al.* (1985)).

In the first part of this paper we repeat, in essence, one of the calculations of FE, but examine also the evolution of the vorticity and vorticity tendency fields. We believe this is necessary to obtain a complete picture of the dynamics. To study the vorticity dynamics we have found it necessary to significantly improve the model resolution. We thought it was desirable also to reformulate the Arakawa–Jacobian representation of the nonlinear terms so that absolute enstrophy is conserved. Both CW's and FE's models conserve only relative enstrophy. In addition, we use a slightly different profile for the initial symmetric vortex to that used by CW and FE since, for parameter values of interest (their $b<1$), their profile has an infinite gradient of relative vorticity at the rotation axis. Unlike FE, we use Kasahara and Platzman's method III to partition the flow between the 'vortex' and the 'environment', the consequences of which are discussed. Finally, we study the relationship between the vortex translation velocity and the mean environmental velocity averaged over selected annuli concentric with the vortex. The latter is a popular technique for computing the environmental speed in observational studies and our aim is to determine the most appropriate size of annulus.

In the second part of the paper we consider the motion of initially asymmetric vortices. The calculations are relevant to the problem of initializing tropical cyclones in numerical forecast models, since cyclones often have pronounced asymmetries, even relative to the motion of their centre (see CW p. 1261 and refs.). Furthermore, they may help ultimately to understand erratic changes in motion due to the development of pronounced internal asymmetries during the forecast period. Finally, the problem of two interacting cyclones is considered briefly as a case of extreme asymmetry.

2. The numerical model

The model is similar to that used by CW and FE. It employs a finite-difference scheme to solve the nondivergent barotropic vorticity equation

$$\partial\zeta/\partial t + u\,\partial\zeta/\partial x + v\,\partial\zeta/\partial y + \beta v = 0 \tag{2.1}$$

over a square domain $-L \leqslant x \leqslant L$, $-L \leqslant y \leqslant L$, on a beta plane. Here u and v are the velocity components in the east ($x-$) and north ($y-$) directions, ζ is the vertical component of relative vorticity, β is the meridional rate of change of the Coriolis parameter, and t is time. Channel boundary conditions ($v = 0$) are imposed at $y = \pm L$ and cyclic boundary conditions are applied at $x = \pm L$. In the solution method, the velocity components are expressed in terms of a streamfunction ψ (i.e. $u = -\psi_y$, $v = \psi_x$), whereupon ψ satisfies the equation

$$\nabla^2\psi = \zeta. \tag{2.2}$$

The principal differences between this model and that used by CW and FE are our use of an explicit (Adams–Bashforth) time-stepping procedure and our modified formulation of the Arakawa–Jacobian. In the latter, the nonlinear and beta terms in (2.1) are combined so that absolute enstrophy is conserved. This is conceptually desirable because the vortex dynamics in the model is governed by the conservation of absolute vorticity expressed by (2.1). However, we found that for the comparatively small grid sizes used here, the differences from calculations that conserve only relative enstrophy are negligible. Our model incorporates a weak biharmonic filter applied at each time step to control aliasing.

Like CW we use a domain size $L = 2000$ km, but our calculations are carried out with a finer grid resolution, mostly 10 km, compared with 20 km used by CW and 40 km used by FE. FE chose a domain size of 4000 km and allowed the domain to move with the vortex so that the latter remained within a grid point of the centre of the domain. Although it is not clear what the dynamical consequences of this procedure are when channel boundary conditions are applied on the north and south boundaries of the domain, FE state that "experiments with moving and stationary grids showed very little difference (less than 1%) in the tracks". Fiorino (1987) reports on test calculations which suggest that for domain sizes smaller than 4000 km, the vortex motion is retarded, while there is little difference (less than 2%) between the tracks over 72 hours for domains of 4000 km and 8000 km. Evidently, if one wishes to accurately represent the largest scales of motion, one must use a domain size comparable with the earth's radius, a result that corroborates the calculations of DeMaria (1987). FE found that the grid spacing of 40 km was acceptable for the purpose of calculating the vortex track over a 72-hour period. While this may be so, we have carried out tests with our own model in which the vorticity tendencies after one and two time steps were compared with the analytic solution obtained using Adem's method (Adem 1956). The comparison showed that in order to adequately resolve the vorticity at this early stage, a much higher spatial resolution than

40 km is required (the tests were carried out using Adem's vortex profile as an initial condition with the radius of maximum tangential wind at 76 km). Since our interest in the present work is to study the evolution of both the vorticity and streamfunction fields, we have been forced to compromise on the domain size to achieve a higher resolution of the vortex core. The compromise is acceptable as we concentrate attention on the first 24 hours of integration when the vortex centre is still relatively far from the domain boundary. During this time the difference in the tracks in calculations for domain sizes 2000 km square and 4000 km square is minimal (Fiorino 1987, Fig. 2.7), although it becomes significant after 72 hours.

As an initial condition for the study in section 4 we use a symmetric vortex profile characterized by the streamfunction ψ given by

$$\psi(s) = -\hat{\psi}/(1 + as^2 + bs^6) \tag{2.3}$$

where $\hat{\psi}$, a and b are constants and $s = r/r_{max}$. This function is continuous and has finite derivatives at $r = 0$. The constants are chosen so that the tangential velocity component $V(r)(=d\psi/dr)$ has the maximum value v_{max} at $r = r_{max}$ (i.e. $dV/ds = 0$ at $s = 1$) and $V = v_o$ at some outer radius r_o. The term s^6 in (2.3) ensures rapid decay of the tangential velocity profile as $s \rightarrow \infty$. Figure 1 compares the profile of $V(r)$ derived from (2.3) with the profile used by CW when $v_{max} = 40\,m\,s^{-1}$, $r_{max} = 100$ km, $v_o = 15\,m\,s^{-1}$ and $r_o = 300$ km. For these values, $a = 0{\cdot}3398$, $b = 5{\cdot}377\times10^{-4}$ and $\hat{\psi} = 1{\cdot}0524\times10^{7}\,m^2s^{-1}$ in (2.3). In the domain of interest the profiles are very similar; however, the profiles used by CW and FE have the undesirable property that, for their parameter $b<1$ (the range of interest), the radial vorticity gradient is infinite along the vortex axis.

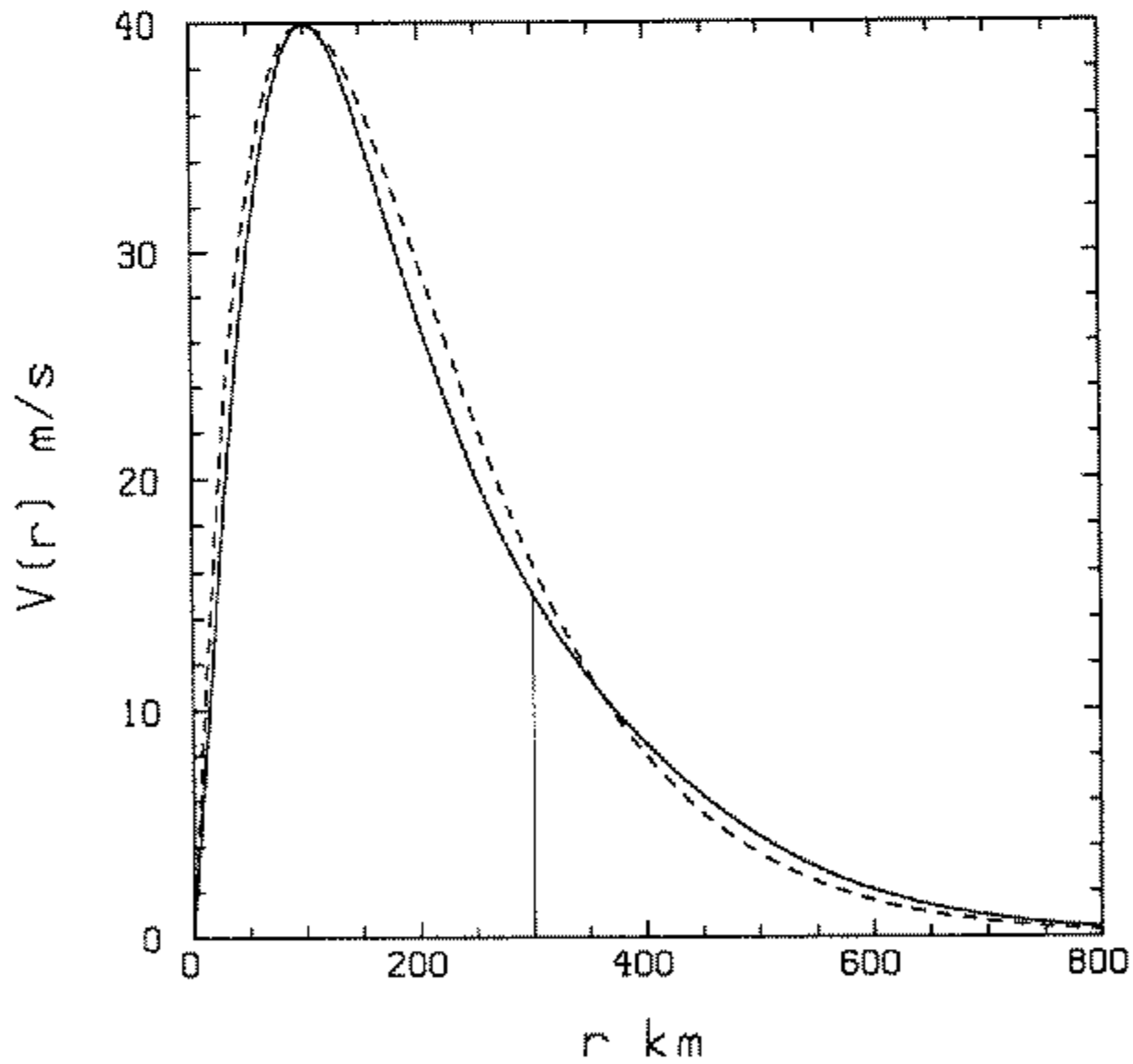

Figure 1. Radial profile of tangential velocity $V(r)$ for the vortex used in this study (solid line). The broken line shows the profile used by Chan and Williams (1987).

3. Flow diagnostics and vortex partitioning

As a means of understanding the vortex motion and of portraying the flow evolution we have chosen a different method of partitioning the flow between the 'vortex' and the 'environment' than that used by FE. They characterized the vortex at each instant as the azimuthal average of the total streamfunction about the streamfunction minimum and

used the latter to define the vortex centre[1]. The residual flow (i.e. the asymmetric component) was *defined* as the environment. In this method of partitioning, the net relative circulation of the vortex about a circuit at large radii becomes increasingly more anticyclonic with time (recall that the circulation is initially zero). This decrease is consistent with a gross decrease in the vortex relative vorticity as the vortex tracks polewards, conserving its absolute vorticity. It means, however, that the streamfunction of the vortex becomes unbounded for $t > 0$ (cf. Kasahara (1957), Eq. (8)) and the vortex so defined is effectively no longer isolated. Following Kasahara and Platzman (1963) we *define* the vortex to be the initial relative vorticity distribution, appropriately located, in which case all the flow change accompanying the vortex motion resides in the residual flow that *defines* the vortex environment. Kasahara and Platzman used a variational principle to determine an 'appropriate location' for the vortex, whereas we have chosen to use the position of the relative vorticity maximum. The method used to determine this is described briefly in appendix A.

It should be emphasized that there is no unique method of partitioning and different methods may have their merits in different applications. We prefer the present method for our study, essentially Kasahara and Platzman's method III, because all the subsequent flow changes are contained in one component of the partition and the vortex remains isolated in the sense described above. Further, one does not have to be concerned with vorticity transfer between the symmetric vortex and the environment as this is zero, by definition. The method has advantages also for understanding the motion of initially asymmetric vortices discussed in section 5.

4. Vortex motion on a beta plane

In this section we re-examine the basic problem of vortex motion on a beta plane with no imposed basic flow, as studied by CW and FE. We choose $\beta = 2{\cdot}23\times10^{-11}\mathrm{m}^{-1}\mathrm{s}^{-1}$, corresponding with latitude 12·5°. Attention is focused on the simultaneous evolution of the asymmetric (i.e. environmental) vorticity and streamfunction fields shown in Fig. 2 for selected times. The prominent feature of these fields is the rapid development of a distorted dipole structure with a vorticity minimum and streamfunction maximum to the north-east of the vortex centre and corresponding maximum/minimum to the south-west. At early times ($t \ll r_{\max}/v_{\max}$) the vorticity dipole is oriented east–west and the maxima and minima thereof occur near the radius of maximum tangential wind speed (Fig. 2(a)). As time proceeds, the dipole axis (the line between the maximum and minimum) rotates counterclockwise, rapidly at first, and the dipole scale (the distance separating the maximum and minimum) steadily increases. The corresponding streamfunction fields (Ψ) show a similar evolution and indicate the rapid development of flow across the vortex centre (denoted by the cyclone symbol in the figures). The motion of the symmetric vortex must be attributed largely to advection by this environmental flow since the vortex cannot advect itself (i.e. $\mathbf{u}\cdot\nabla\zeta \equiv 0$ for a symmetric vortex) and propagation of the centre in the form of planetary wave motion is negligible (CW, p. 1260). Further evidence for this assertion is given below.

The vortex track during a 72-hour integration is shown in Fig. 3. The track is essentially the same as that shown in CW (Fig. 6). Note that during the first 12 hours, the displacement of the vortex centre is small compared with the dipole scale of the gyres in Fig. 2. This suggests that insight into the gyre structure may be obtained by considering a simple symmetric vortex flow $V(r)$ on a beta plane in which the vortex is held fixed. If

[1] In general, and even in the special case of a symmetric vortex translating steadily without change of form in a uniform flow on an f plane, the streamfunction minimum and vorticity maximum are *not* co-located.

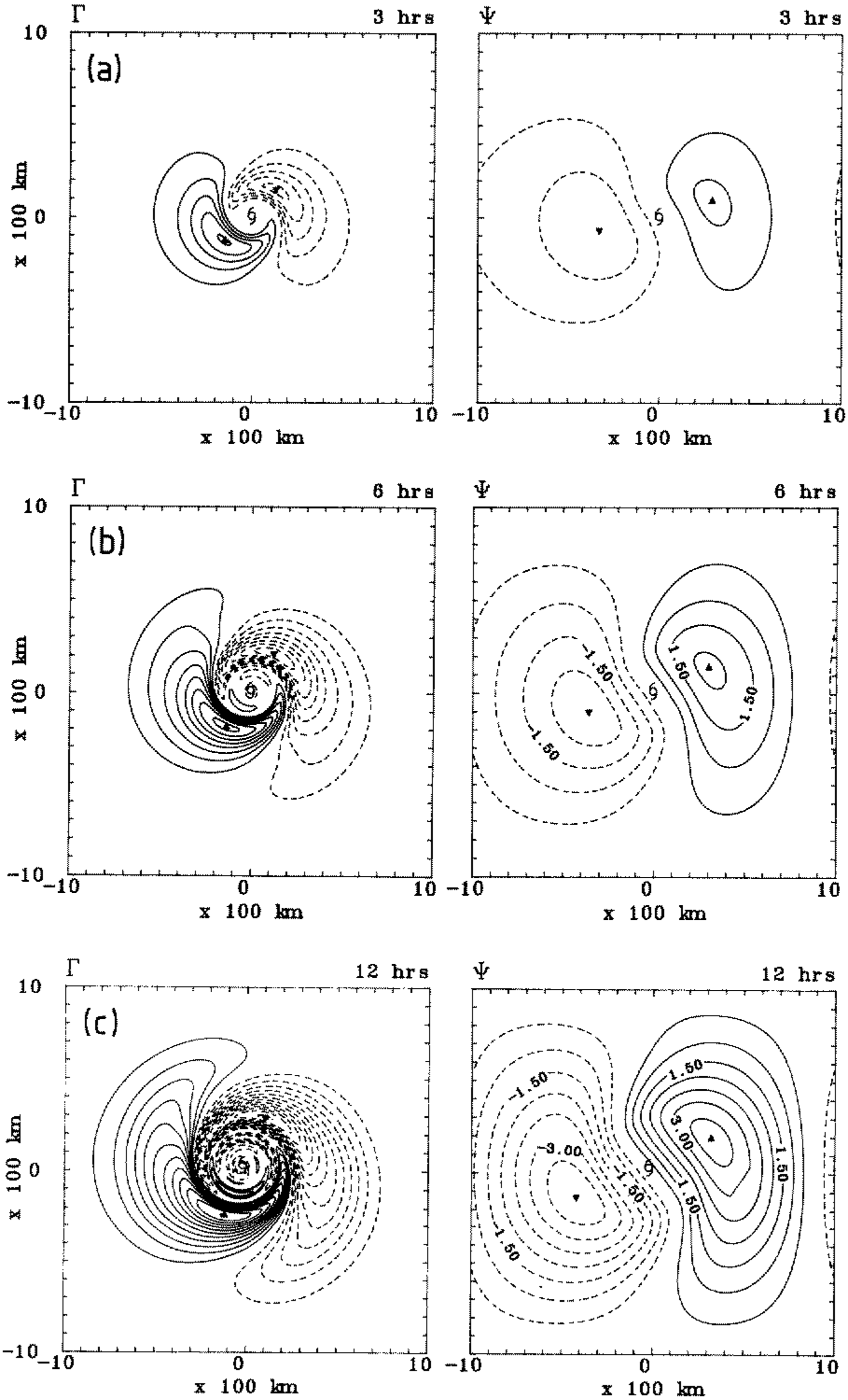

Figure 2. Evolution of the environmental (i.e. asymmetric) vorticity (Γ) and streamfunction (Ψ) fields associated with the motion of a symmetric vortex on a beta plane. The vortex centre is marked by a tropical cyclone symbol. Solid triangles mark the location of the maxima and minima of the fields. Times shown are: (a) 3 hours; (b) 6 hours; (c) 12 hours; (d) 24 hours; and (e) 48 hours. Contour intervals for Γ are $1{\cdot}0\times10^{-6}s^{-1}$ in (a)–(c) and $5{\cdot}0\times10^{-6}s^{-1}$ in (d) and (e); contour intervals for Ψ are $5{\cdot}0\times10^{4}m^{2}s^{-1}$ in (a)–(d) and $10^{5}m^{2}s^{-1}$ in (e). The zero contours have been excluded. (Continued overleaf.)

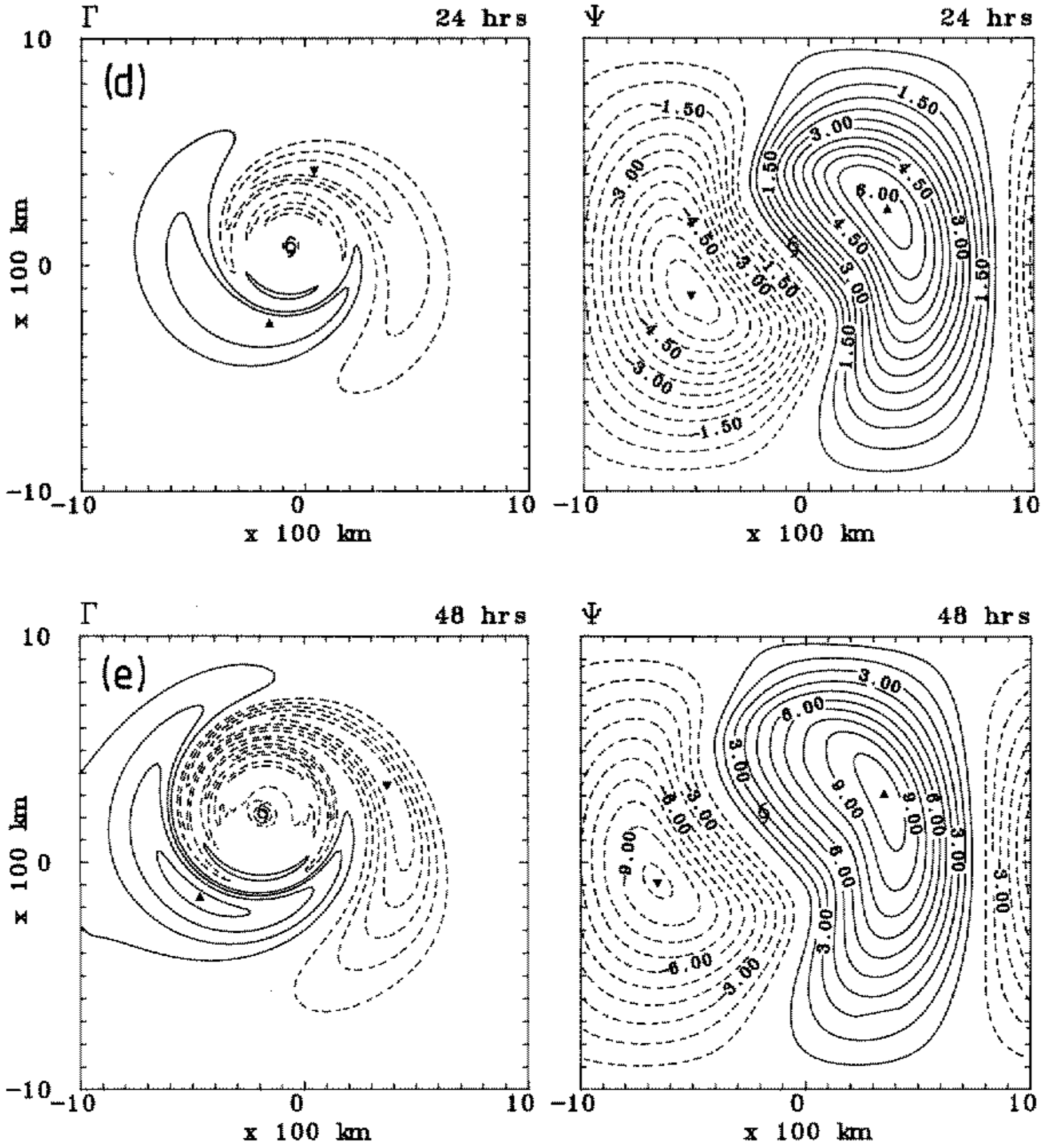

Figure 2 (continued)

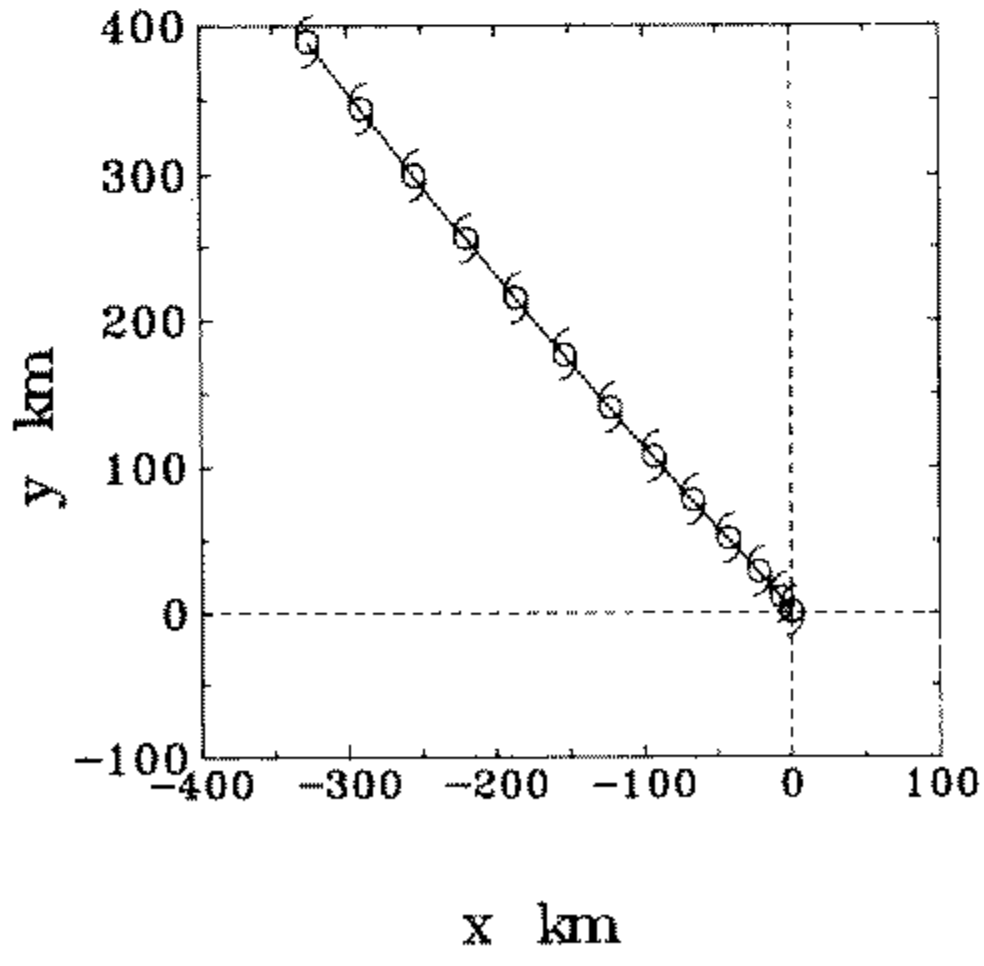

Figure 3. Vortex track based on the motion of the vorticity maximum. Cyclone symbols denote vortex positions at six-hour intervals to 72 hours. The origin of coordinates is the initial position.

the vortex is 'suddenly imposed' at $t = 0$, as in the numerical model, the asymmetric vorticity ζ_a at the point (x, y) at time t is

$$\zeta_a(x, y, t) = -\beta(y - y_o) \tag{4.1}$$

where y_o is the meridional coordinate of the initial position of the fluid particle now at (x, y). In polar coordinates (r, θ), (4.1) may be written

$$\zeta_a = -\beta r(\sin\theta - \sin\theta_o) \tag{4.2}$$

where

$$\theta_o = \theta - \Omega(r)t \tag{4.3}$$

and $\Omega(r) = V(r)/r$ is the angular velocity of an air parcel around the vortex. Figure 4 shows the asymmetric vorticity distribution given by (4.2) for the vortex characterized by Eq. (2.3) at 3, 6 and 24 hours, together with the corresponding streamfunction distributions ψ_a. The latter are obtained by solving Eq. (2.2) with ζ_a on the right-hand side, using the same boundary conditions as in the numerical model. Comparison of Fig. 4 with the corresponding panels of Fig. 2 shows that at early times ($t \leqslant 6$ hours), there is good agreement between the asymmetric vorticity patterns and, although this agreement deteriorates with time, it is still remarkable at 24 hours. Similar remarks apply to the streamfunction field. For the vortex profile we have used, the actual differences are partly attributable to the fact that the planetary wave modes associated with the advection of planetary vorticity by the environment have a westward phase propagation. This does not occur in the stationary vortex calculation expressed by (4.2) and (4.3) since the advection of planetary vorticity by the asymmetric flow is not taken into account. The westward propagation is especially evident in Figs. 2(d) and (e), where the region of negative streamfunction has re-entered the domain from the east. Note that the westward speed of the gravest planetary wave mode in the domain is 86 km/d. Other differences are associated with the vortex movement.

The positions of the extrema in the asymmetric vorticity pattern ζ_a are determined by the conditions $\partial\zeta_a/\partial\theta = 0$ and $\partial\zeta_a/\partial r = 0$. Using (4.2) and (4.3), the former condition gives

$$\theta = \tfrac{1}{2}\Omega(r)t = \theta_*(r, t) \tag{4.4}$$

whereupon the latter condition gives

$$\tan\theta_* + r\,\partial\theta_*/\partial r = 0. \tag{4.5}$$

Equation (4.5) is a transcendental equation for r as a function of time, say $r_*(t)$. Given the functional form of $\Omega(r)$, Eq. (4.5) is readily solved using the Newton–Raphson iteration method. Figure 5 compares the angular and radial positions of the maximum and minimum values of ζ_a, and the magnitude of these extrema, with the corresponding quantities in the full numerical calculation. The agreement between the radial positions is excellent up to 24 hours and the angular positions θ_* are reasonably well predicted during this time, although they are slightly overestimated by the analytic calculations. Beyond 24 h there are large discrepancies between the numerical and analytic calculations, where, for example, in the former, the minimum in the asymmetry retrogresses sharply, before stabilizing at about 15° at 48 h. Inspection of the vortex asymmetry patterns beyond 24 h (see e.g. Fig. 2(e)) suggests that the vortex motion rapidly becomes an important factor in their subsequent evolution.

The breakdown of the analysis represented by (4.2) and (4.3) can be expected to occur when $r_*(t)$ is such that $V(r_*)$ is no longer large compared with the northward component of the vortex centre velocity, **c**. Accordingly, the rapid retrograde movement

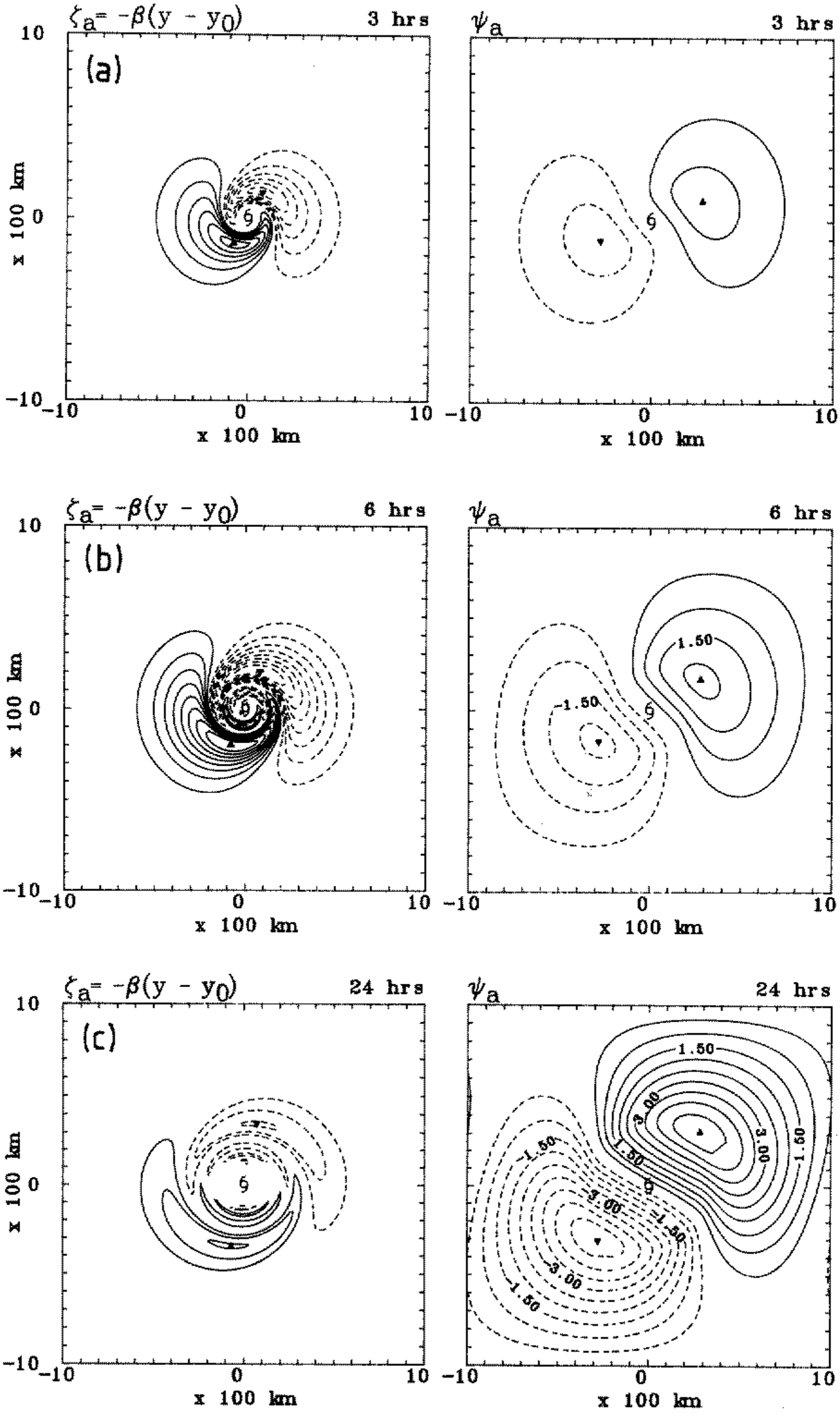

Figure 4. Evolution of the asymmetric vorticity field (ζ_a) and the corresponding streamfunction field (Ψ_a) calculated for the same symmetric vortex as used in Fig. 2, but on the assumptions that the vortex remains stationary and the advection of absolute vorticity is by the symmetric velocity field only. Shown are the fields at 3, 6 and 24 hours. For comparison, the contour intervals and symbols are the same as those in Fig. 2. Again, the zero contours have been excluded.

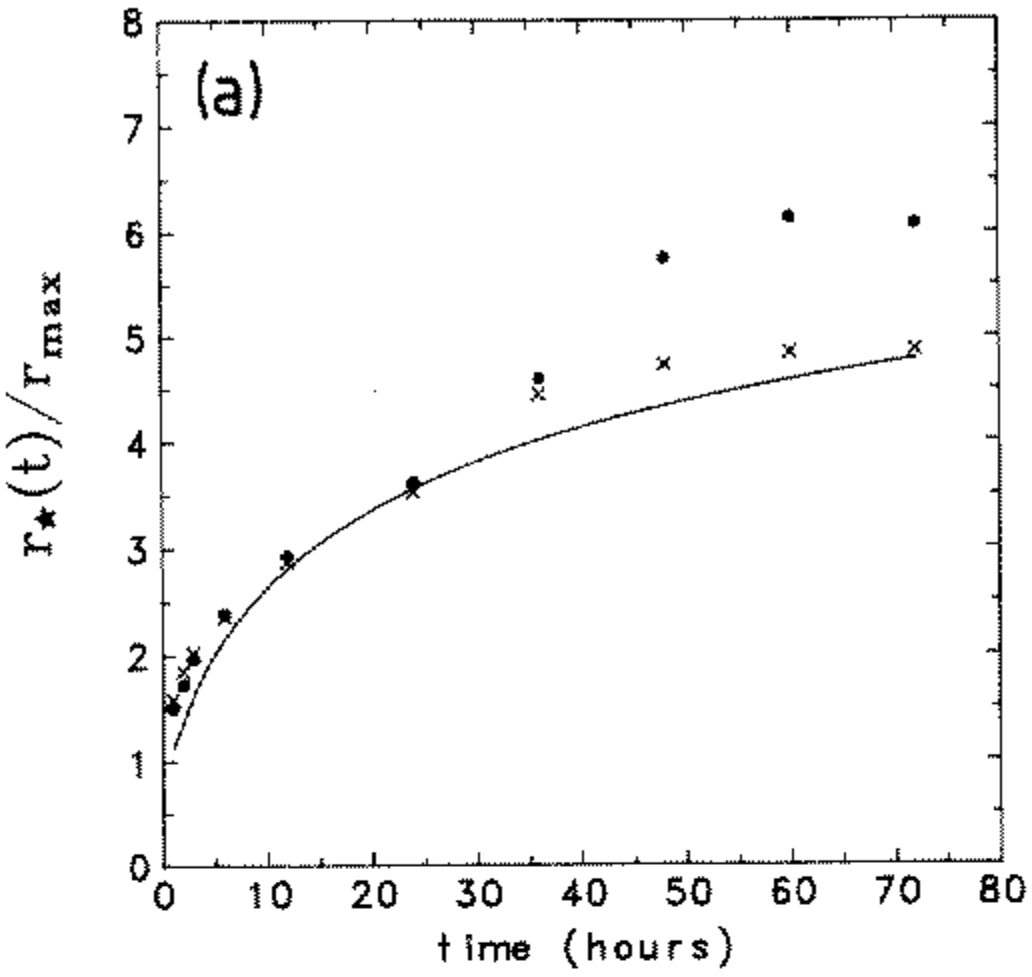

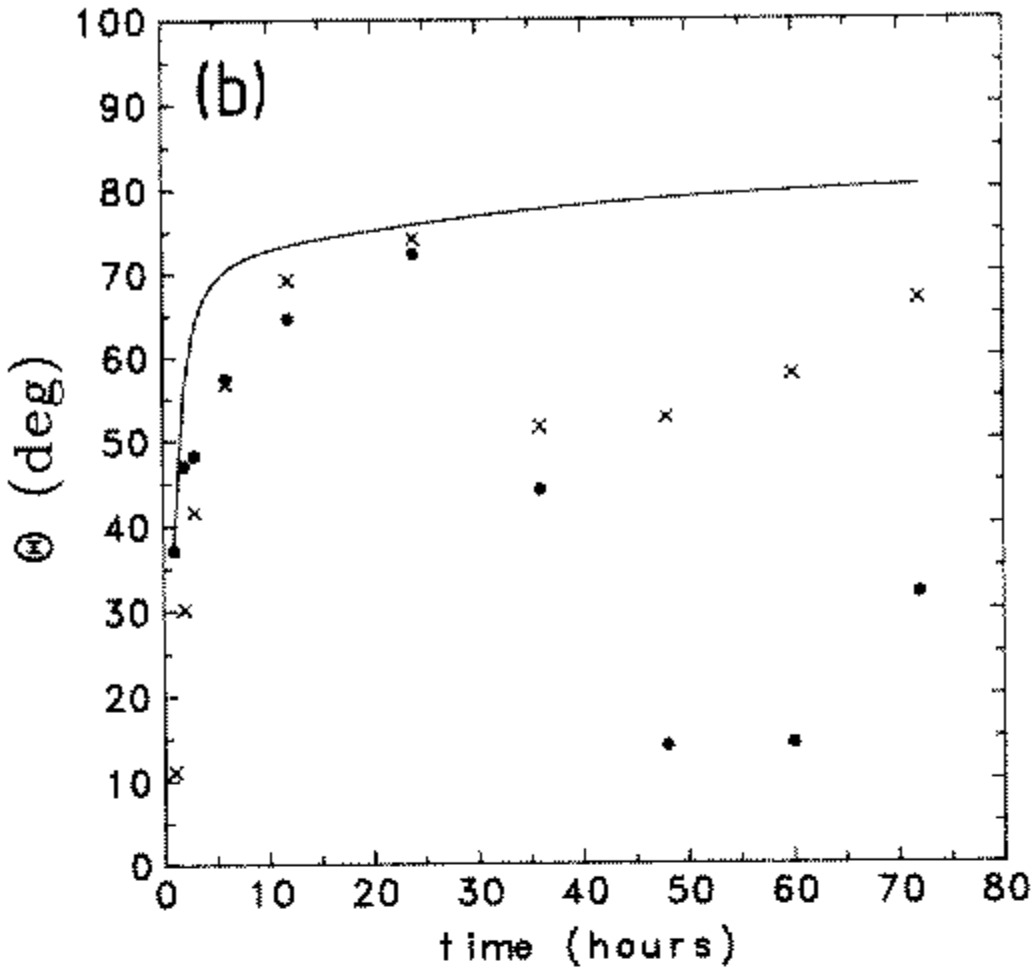

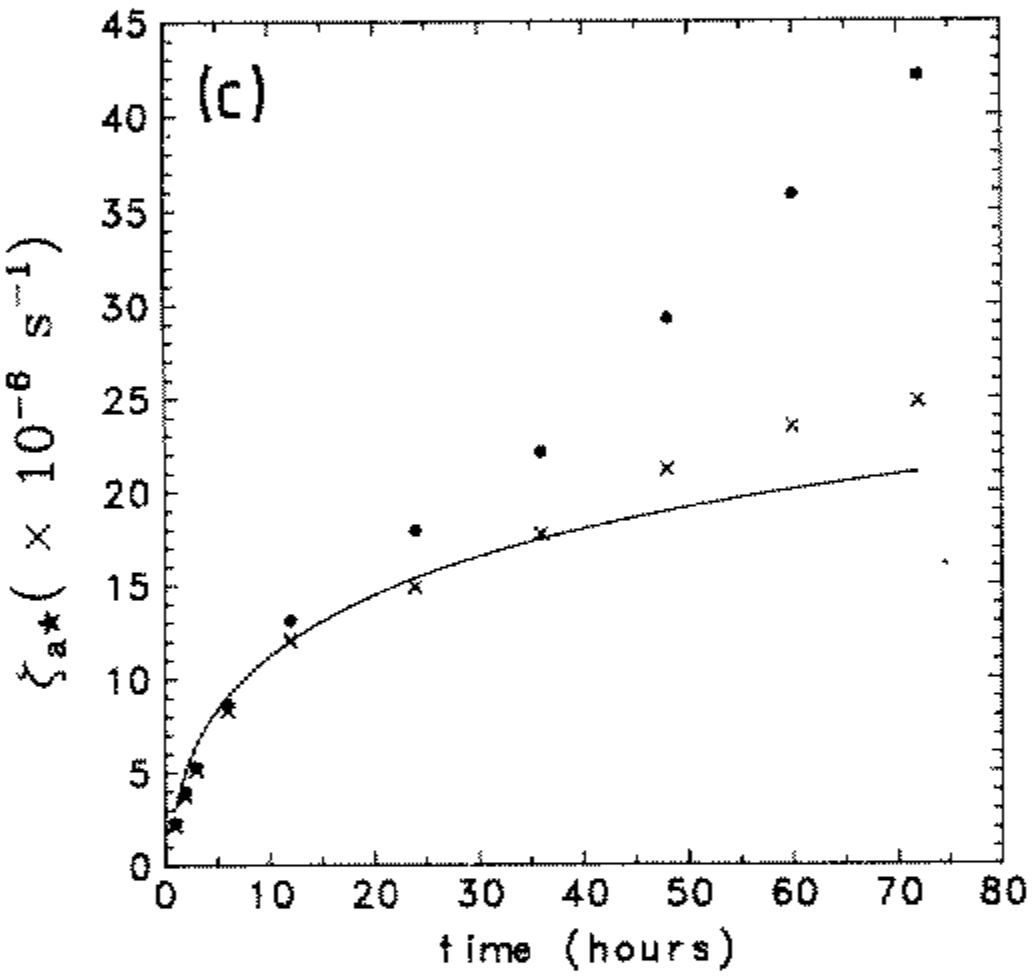

Figure 5. Time evolution of the asymmetric gyre structure in the full numerical calculation of vortex motion on a beta plane (points) compared with the analytic predictions (full line) for the stationary vortex calculation (Fig. 4) characterized by: (a) the radius of the vorticity extrema in units of r_{max}; (b) the angle subtended by the vorticity extrema from the vortex centre relative to the eastward direction; and (c) the magnitude of the vorticity extrema in units of $10^{-6}s^{-1}$. The crosses denote maxima and the dots minima.

of the vorticity minimum after 24 hours is associated with the decline of $V(r)$ to values of less than $10\,m\,s^{-1}$ for $r > 400\,km$. At these radii, air parcel trajectories relative to the moving vortex centre can be expected to deviate significantly from circles. Figure 5(c) shows that after 24 h, the magnitude of the asymmetric vorticity minimum increases dramatically in comparison with the prediction of (4.2) and (4.3) and this is presumably associated with the more distant position of the minimum from the vortex centre. It would be possible to check this association by computing selected air parcel trajectories. However, we doubt that this would yield significant further insight into the gyre evolution to warrant the computational effort involved.

FE sought to analyse the flow evolution by calculating the separate contributions of individual terms in the streamfunction tendency equation. In the present paper we examine the analogous contributions to the vorticity equation. As noted earlier, this equation could be regarded as being more fundamental, even though in real cyclones, the vorticity field is much more difficult to determine, requiring differentiation rather than an integration of the observed wind field.

In the Kasahara–Platzman partition method, the vorticity tendency equations for the vortex and the environment are, respectively,

$$\partial \zeta_{sym}/\partial t = -\mathbf{c}\cdot\nabla\zeta_{sym} \tag{4.6}$$

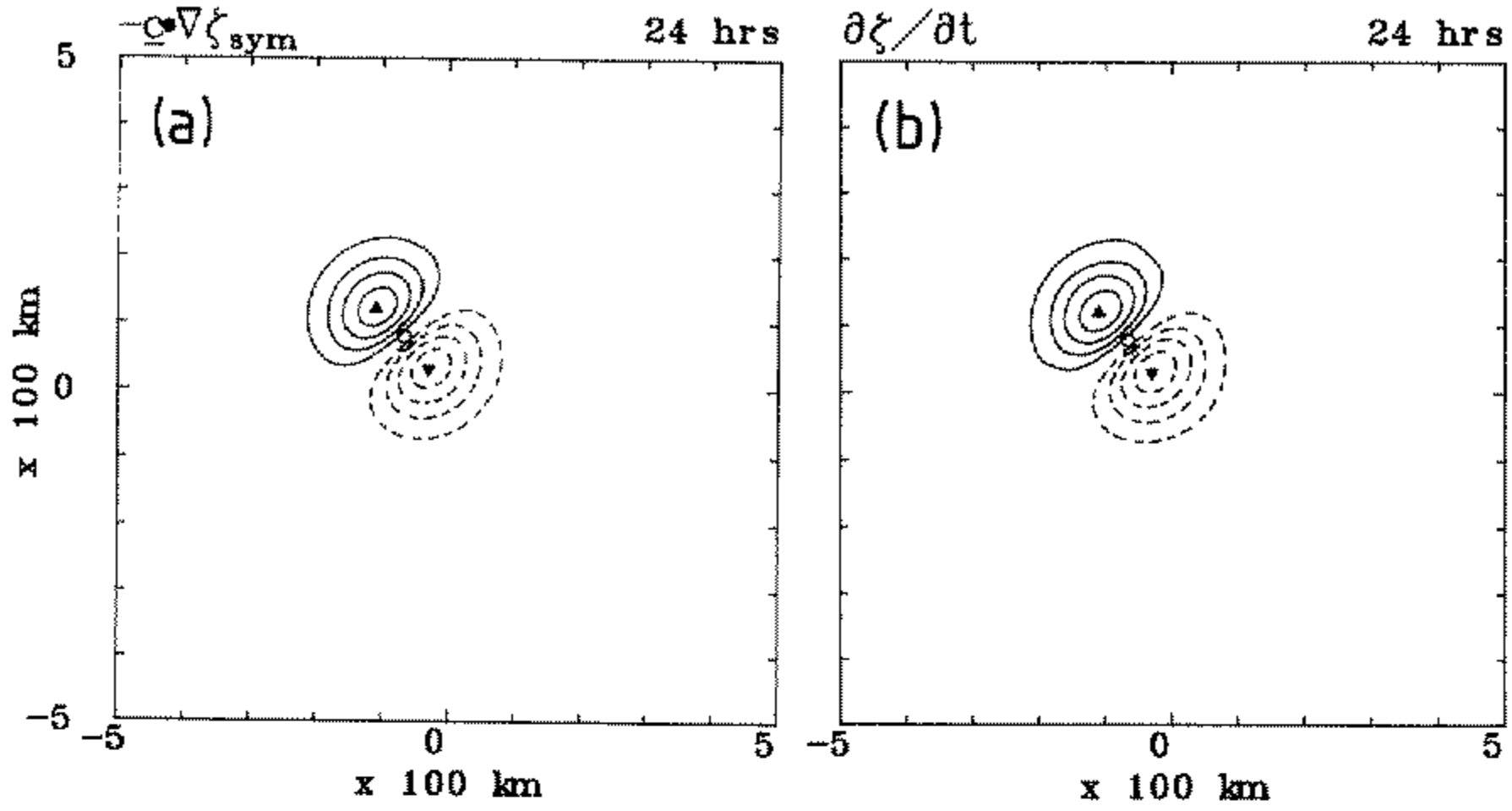

Figure 6. Isolines of vorticity tendency: (a) due to the term $-\mathbf{c}\cdot\nabla\zeta_{sym}$ in Eq. (4.6) compared with, (b) the total vorticity tendency $\partial\zeta/\partial t$ in Eq. (2.1) at 24 hours. Contour interval is $5{\cdot}0\times10^{-9}s^{-2}$. Zero contours have been excluded.

and

$$\partial\Gamma/\partial t = -(\mathbf{U}-\mathbf{c})\cdot\nabla\zeta_{sym} - \mathbf{u}\cdot\nabla\Gamma - \mathbf{U}\cdot\nabla\Gamma - \mathbf{u}\cdot\nabla f - \mathbf{U}\cdot\nabla f \qquad (4.7)$$

where $\mathbf{u}$ and $\mathbf{U}$ are the partitioned wind vectors of the vortex and the environment, ζ_{sym} is the vortex vorticity and $\Gamma = \zeta - \zeta_{sym}$ is the environmental vorticity. As noted in section 3, we define the vortex velocity $\mathbf{c}$ as the translation velocity of the relative vorticity maximum. Diagnostic fields of various terms in Eqs. (4.6) and (4.7) at 24 hours are shown in Figs. 6, 7 and 9 for a subdomain of the flow, and an interpretation of these now follows.

Figure 6 shows the advection term on the right-hand side of (4.6) and compares it with $\partial\zeta/\partial t$, the calculated tendency of the *total* vorticity obtained from the finite-difference form of (2.1). For the contour levels chosen, these fields are virtually the same, showing that at lowest order the vorticity changes are simply a reflection of the vortex motion. The environmental vorticity tendencies shown in Fig. 7 are at least an order of magnitude less than the advective tendency $-\mathbf{c}\cdot\nabla\zeta_{sym}$ in (4.6) and reflect the diversity of scales involved in tropical cyclone motion (Kasahara and Platzman 1963, p. 323[2]).

To assist in the interpretation of parts of Fig. 7 we show in Fig. 8 the streamlines and isotachs of the environmental flow relative to the moving vortex, i.e. $\mathbf{U}-\mathbf{c}$. Referring to the latter figure and to the streamfunction pattern in Fig. 2(d), we note that the environmental streamflow is appreciably uniform on the scale of the vortex (i.e. at least $2r_{max}$) and the vortex moves with a velocity that is very close to that of the environmental flow across its centre. Indeed, the relatively small nonzero value of $|\mathbf{U}-\mathbf{c}|$ at the vortex centre is probably as much a reflection of the inevitable numerical inaccuracies in computing $\mathbf{U}$ and $\mathbf{c}$, as any physical effect, e.g. propagation through planetary wave dispersion.

We return now to an interpretation of Fig. 7, which shows the contributions to $\partial\Gamma/\partial t$ as follows:

[2] We note in passing a misleading conclusion from this scale analysis which suggests that $\mathbf{u}\cdot\nabla_{sym}$ is the largest term in the equation; however, for a symmetric vortex, this term is identically zero because the two vectors are perpendicular.

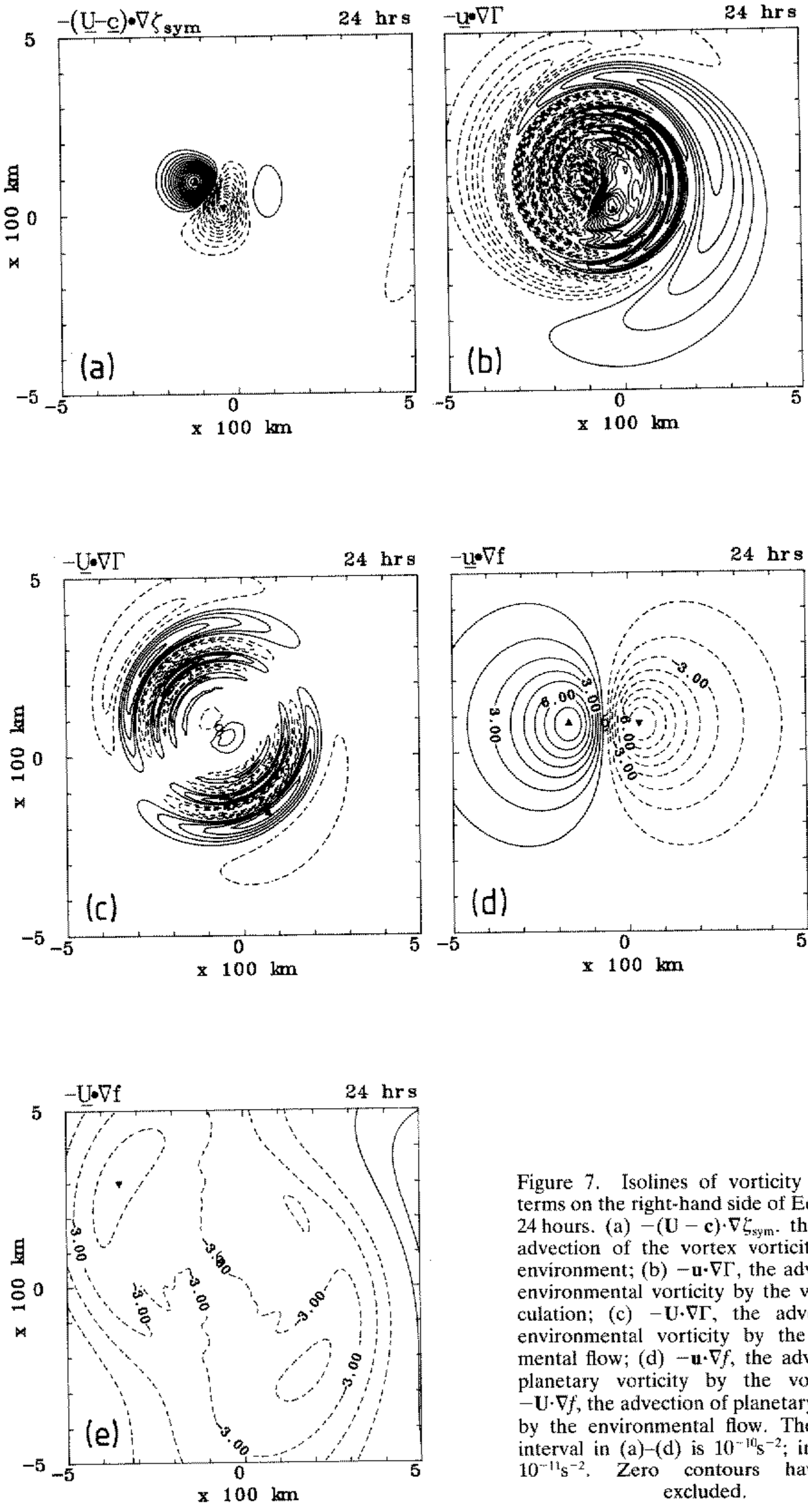

Figure 7. Isolines of vorticity tendency terms on the right-hand side of Eq. (4.7) at 24 hours. (a) $-(\mathbf{U}-\mathbf{c})\cdot\nabla\zeta_{sym}$. the relative advection of the vortex vorticity by the environment; (b) $-\mathbf{u}\cdot\nabla\Gamma$, the advection of environmental vorticity by the vortex circulation; (c) $-\mathbf{U}\cdot\nabla\Gamma$, the advection of environmental vorticity by the environmental flow; (d) $-\mathbf{u}\cdot\nabla f$, the advection of planetary vorticity by the vortex; (e) $-\mathbf{U}\cdot\nabla f$, the advection of planetary vorticity by the environmental flow. The contour interval in (a)–(d) is $10^{-10}s^{-2}$; in (e) it is $10^{-11}s^{-2}$. Zero contours have been excluded.

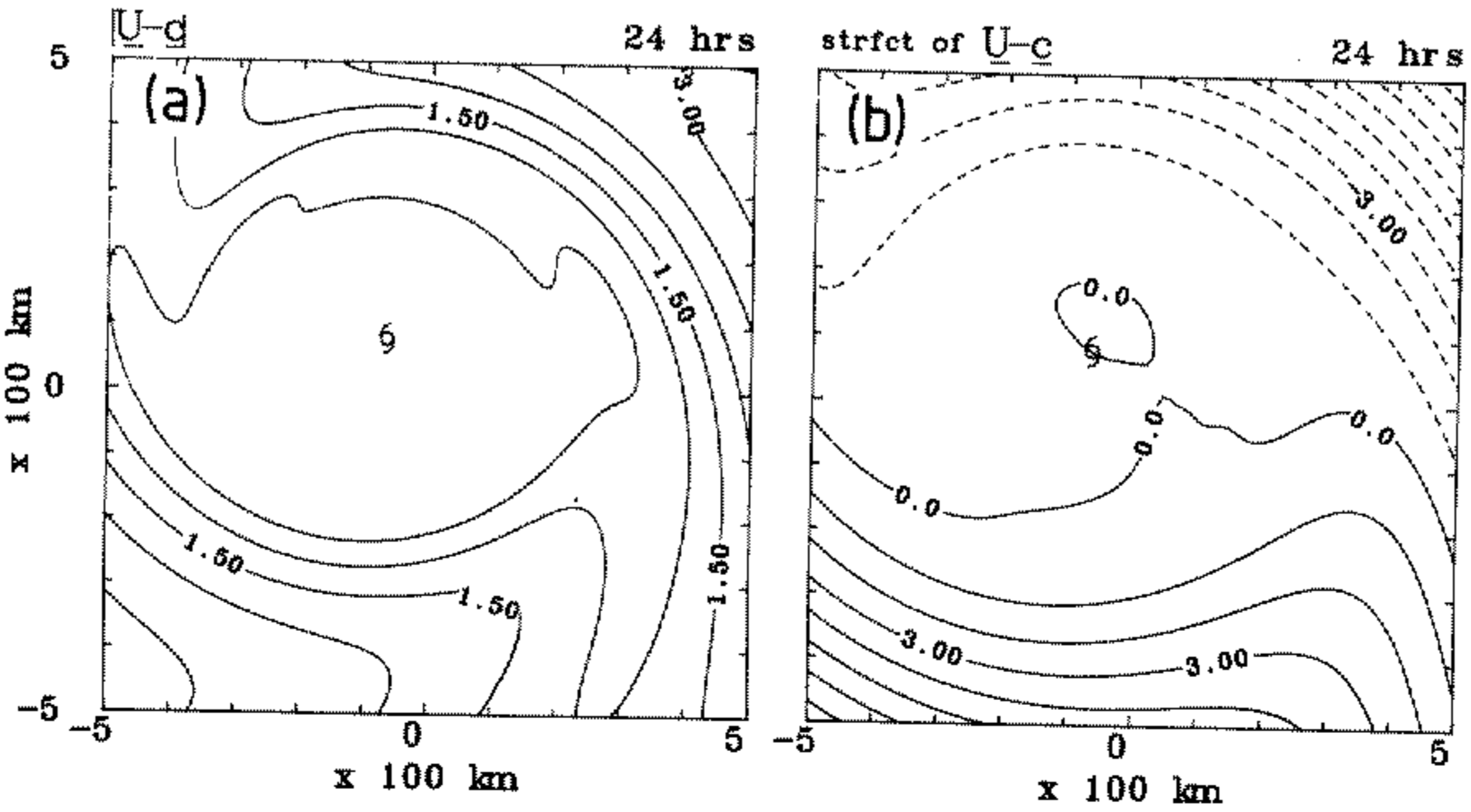

Figure 8. Isotachs (a) and streamlines (b) of the environmental flow *relative to the moving vortex* at 24 hours. Contour interval is $0{\cdot}5\,\mathrm{m\,s^{-1}}$ in (a) and $10^5\mathrm{m^2s^{-1}}$ in (b). The cyclone symbol indicates the vortex centre where the computed isotach minimum is less than $0{\cdot}01\,\mathrm{m\,s^{-1}}$.

(i) $-(\mathbf{U}-\mathbf{c})\cdot\nabla\zeta_{\mathrm{sym}}$. This term represents the advection of vortex vorticity by the vortex relative flow and has a pattern similar to that in Fig. 6(a). However, the precise magnitudes of the maxima and minima are sensitive to the diagnosis of **c**. The term is always zero at the vortex centre because $|\nabla\zeta_{\mathrm{sym}}| = 0$ there, but it would be zero elsewhere where $\mathbf{U} = \mathbf{c}$. Since $|\nabla\zeta_{\mathrm{sym}}|$ has a maximum of $1{\cdot}37\times10^{-8}\mathrm{m^{-1}s^{-1}}$, an error of $0{\cdot}1\,\mathrm{m\,s^{-1}}$ in calculating $\mathbf{U}-\mathbf{c}$ will lead to a maximum error in calculating $|(\mathbf{U}-\mathbf{c})\cdot\nabla\zeta_{\mathrm{sym}}|$ on the order of $10^{-9}\mathrm{s^{-2}}$ which is comparable with the maximum of $1{\cdot}5\times10^{-9}\mathrm{s^{-2}}$ in Fig. 7(a). Since $0{\cdot}1\,\mathrm{m\,s^{-1}}$ would be an acceptable error in the calculation of **c**, care should be taken not to attribute too much significance to the magnitude (and sign) of this pattern. Again, the foregoing problem is a reflection of the diverse scales involved in cyclone motion.

(ii) $-\mathbf{u}\cdot\nabla\Gamma$. This term represents the advection of the environmental vorticity, essentially the asymmetric vorticity in this problem, by the vortex circulation. It has a maximum magnitude of $1{\cdot}8\times10^{-9}\ \mathrm{s^{-2}}$ and makes an important contribution to (4.7). Because the angular velocity of the vortex $\Omega(r)$ decreases with radius (see section 5), such advection effectively shears out the vorticity asymmetry, winding it round and round the core as discussed earlier. Accordingly, this effect leads progressively to fine scale structure in the vorticity field and thereby to the inability of a numerical scheme to adequately resolve it!

(iii) $-\mathbf{U}\cdot\nabla\Gamma$. This term represents an advection of the asymmetric vorticity field by the environmental flow. The maximum absolute magnitude is $5{\cdot}7\times10^{-10}\mathrm{s^{-2}}$, less than one third that of the previous term, but again, the tendency has fine scale structure, reflecting that of the vortex asymmetry.

(iv) $-\mathbf{u}\cdot\nabla f$. This term represents the advection of planetary vorticity by the vortex. It induces an east–west-oriented wavenumber-one asymmetry in the vorticity field, as noted by many previous authors, and has a maximum magnitude $9{\cdot}0\times10^{-10}\mathrm{s^{-2}}$, comparable with the previous terms.

(v) $-\mathbf{U}\cdot\nabla f$. This term represents the advection of planetary vorticity by the environmental flow and although smaller in maximum absolute magnitude (i.e. $4{\cdot}5\times10^{-11}\mathrm{s^{-2}}$) than the other terms, it is important at larger distances from the vortex. Indeed, it is a necessary component for the propagation of Rossby-wave modes in the flow domain.

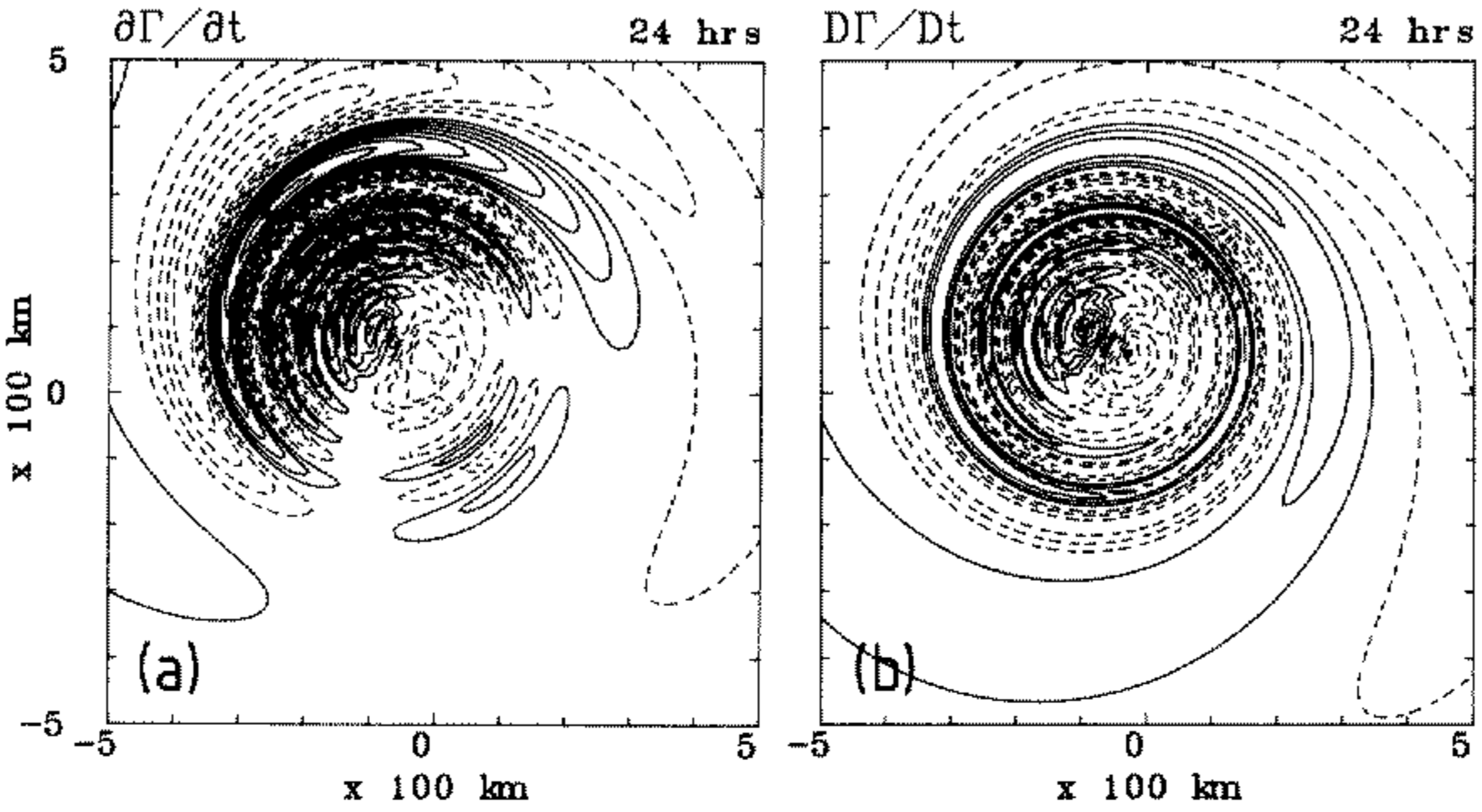

Figure 9. Isolines of (a) $\partial\Gamma/\partial t$, the environmental vorticity tendency, and (b) $D\Gamma/Dt = \partial\Gamma/\partial t + \mathbf{c}\cdot\nabla\Gamma$, the environmental vorticity tendency relative to the moving vortex, at 24 hours. Contour interval is $10^{-10}s^{-2}$.

Figure 9(a) shows the isolines of $\partial\Gamma/\partial t$, the sum of the individual contributions in Fig. 7, while Fig. 9(b) shows the environmental vorticity tendency relative to the moving vortex, $\partial\Gamma/\partial t + \mathbf{c}\cdot\nabla\Gamma$. A prominent feature of both these fields is the relatively fine scale structure, dominated in the latter case by the advection of asymmetric vorticity by the vortex (term (ii) above). The small-scale gyre structure in the vortex core region is dominated by the contribution of term (i) and is almost certainly a result of numerical inaccuracy (see the above discussion).

The foregoing analysis complements FE's study, which concentrates solely on the streamfunction and streamfunction tendencies and which uses a different and, in our view, less easily interpretable partitioning scheme for the analysis. It highlights a number of important features of the vorticity dynamics which may be summarized as follows:

(1) The close similarity of the numerically and analytically computed asymmetric vorticity fields for $t \leqslant 24$ h suggests that, at least for the vortex profile under study, the asymmetry is attributable mainly to the advection of the initial absolute vorticity distribution by the (symmetric) vortex circulation (see for example Figs. 2(d) and 4(c)). This asymmetry is essentially wavenumber-one and constitutes a vortex dipole, the maxima and minima of which lie outside the radius of maximum tangential wind speed and separate with time. The cautionary note concerning the particular vortex profile used is necessary because we have found that for initial vortex profiles where the decay of tangential velocity with radius is appreciably larger than in the present case, the asymmetry appears to suffer significant retrograde propagation around the vortex, possibly as a centrifugal wave mode. This effect is being further studied and the results will be reported elsewhere.

(2) The asymmetric vorticity distribution is rapidly reduced to finer and finer scales by the angular shear of the vortex in combination with, especially at later times, the vortex motion. The region of fine scale structure expands with time and has a radial extent on the order of $3r_{max}$ (i.e. 300 km) at 24 h. Significantly, the amplitude extrema of the asymmetric vorticity occur outside these radii. This, together with the fact that fine-scale structure in the vorticity field has a cancelling effect in respect of its contribution to the streamfunction (see e.g. appendix B) explains why the vortex structure at radii beyond 300 km is of crucial importance in vortex motion (FE, p. 15).

(3) The vortex motion as characterized by the motion of the vorticity centre can be

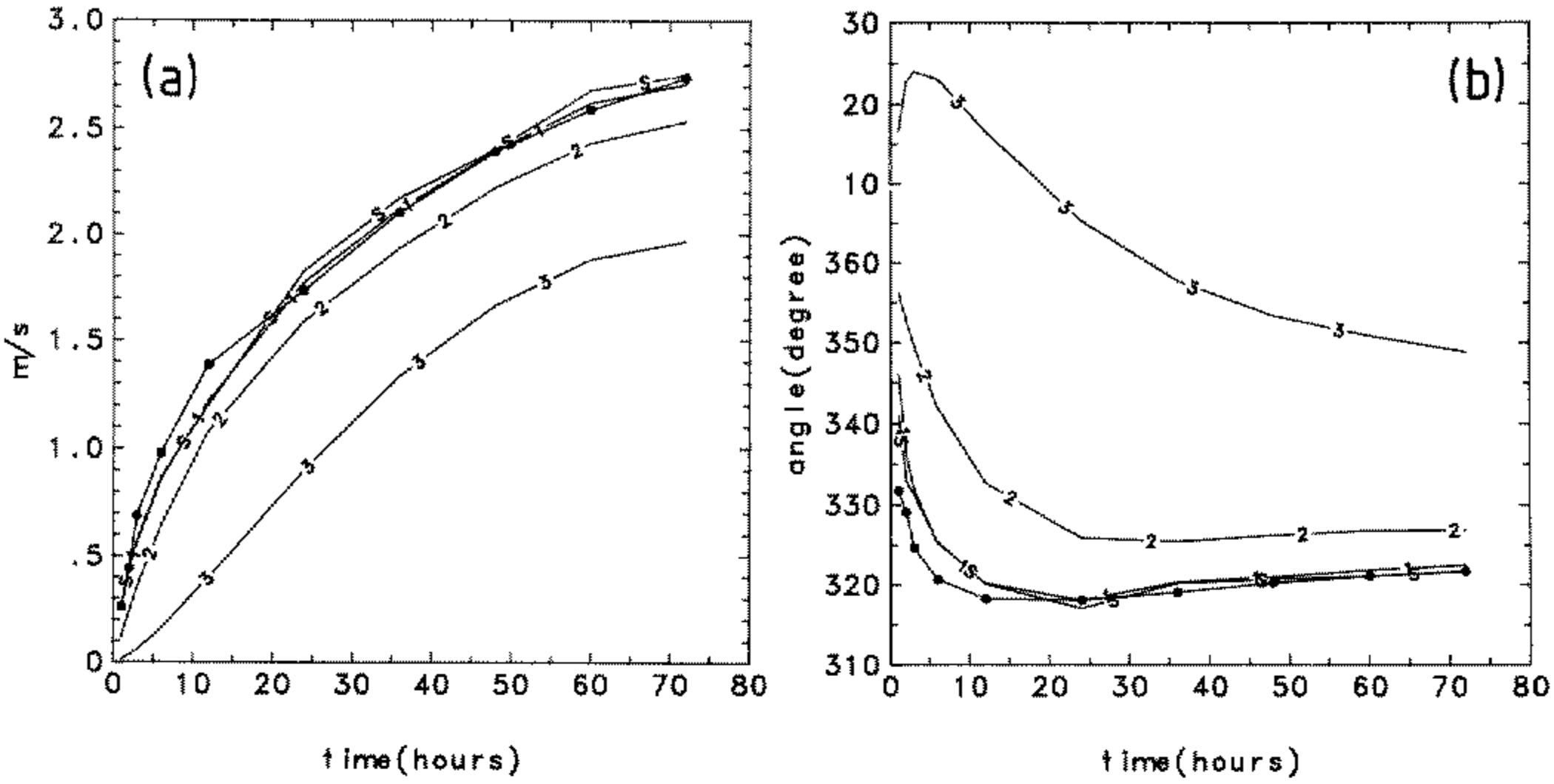

Figure 10. Calculated speed (in $m\,s^{-1}$) and heading of the vortex centre as functions of time (solid line joining dots) compared with the speed and direction computed from the environmental streamfunction at the vortex centre (curve labelled S), and averages of this streamfunction over annuli with radii 0 to 1° latitude (0–111 km)—curves labelled 1; 1–3° latitude (111–333 km)—curves labelled 2, and 3–5° latitude (333–555 km)—curves labelled 3.

attributed to within a close approximation to advection by the environmental flow across the vortex centre when the present partition method is employed. This is consistent with the case of motion of a symmetric vortex in a uniform flow on an f plane, and with expectations from theory, but is contrary to FE's diagnostics. FE find that the vorticity centre translates more slowly than the asymmetric flow in the inner region. It seems likely that this is a consequence of their larger mesh length, which is four times that used in the present calculation.

The general paucity of data in and around tropical cyclones makes it impossible to determine the environmental flow across the cyclone centre with the high resolution provided by the foregoing numerical simulation. Indeed, in order to define an environmental current from observed wind data, for example, it is necessary to average over a considerable area surrounding the cyclone, even in studies using composite data. In the latter case, George and Gray (1976) use an average over an annular region 1–7° latitude in radial extent centred on the storm, while Chan and Gray (1982) use an annular region from 5–7° latitude. The numerical simulation provides an effective means of assessing the applicability of these or other averages in defining an appropriate environmental current. Accordingly we have calculated the environmental wind vector averaged over annular regions from 0–1°, 1–3°, 3–5° and 5–7° latitude[3], centred on the vorticity centre, and have compared these with the environmental flow calculated at the vorticity centre, and with the speed of the centre itself. The results are displayed in Fig. 10 which shows the speed and heading of these various averages except the latter (the one used by Chan and Gray) which turned out to give a rather poor representation of the flow across the vortex centre. For most of the simulation, and certainly after the first 12 hours, the speed and direction of the vortex centre are very well represented both by the environmental velocity vector at the centre calculated directly from the streamfunction and by the average in the circular domain of radius 1° latitude. This would be expected from the uniformity of the environmental streamfunction on the scale of the vortex core as shown

[3] Recall 1° latitude = 111 km.

above. As the size of the annular region is increased, the agreement becomes progressively poorer and the vortex motion has an increasing westward bias relative to the average environmental flow. Again, that this should be so is immediately evident from an inspection of the environmental streamfunction fields in Fig. 2. At the same time, the annular average speed decreases relative to that of the vortex. These results have important implications: they are evidence that the westward drift relative to the environmental flow deduced in some observational studies may be as much a reflection of the particular definition of the environmental flow as of a particular physical effect (e.g. beta drift).

5. Motion of asymmetric vortices

In section 4, following all previous studies, the initial vortex was assumed to be symmetric. Nevertheless, as remarked in section 1, it is known that tropical cyclones often exhibit marked asymmetries, even when flow fields are computed relative to the moving vortex centre[4]. Notwithstanding this, even forecast models, including the barotropic forecast model SANBAR (see Sanders *et al.* 1980 and refs.), assume the initial vortex to be symmetric. The results of section 4 show, however, that flow asymmetries, whether or not they are considered a part of the vortex, have an important effect on the vortex motion. In this section we study the motion of initially *asymmetric* vortices on an f plane and on a beta plane. The issues to be addressed are relevant to the problem of initializing tropical cyclone forecast models as well as to an understanding of possible track changes as cyclones develop new asymmetries. The latter may be associated with the growth of new convective cloud bands in regions of inertia–gravity-wave-induced convergence, for example.

The asymmetric vortices to be studied are constructed by adding a vortex dipole to the initial vorticity distribution derived from (2.3). The vortex dipole has the form

$$\zeta_d(r,\theta) = \zeta_D (r/d)^2 \exp(-r^2/d^2)\cos(\theta - \alpha) \tag{5.1}$$

where ζ_D, d and α are prescribed constants characterizing the dipole strength, scale and orientation. Thus the vorticity maximum and minimum of the dipole occur at (d, α) and $(d, \pi + \alpha)$, respectively.

Four main calculations are described; these are designated S1–S4. In each of these $\alpha = 0$; i.e. the dipole is oriented west–east. In the prototype calculation, S1: $d = \sqrt{2}$; $\zeta_D = 0{\cdot}2\zeta_o$, where ζ_o is the maximum vorticity of the symmetric vortex defined by (2.3); and $\beta = 0$. In S2, $d = 2\sqrt{2}$, but $\zeta_D = 0{\cdot}1\zeta_o$ so that the velocity at the origin associated with the dipole is the same as in S1 (see appendix B, Eq. (B8)). Again $\beta = 0$. The calculations S3 and S4 are repeats of S1 and S2 on a beta plane with the same value for β as used earlier.

Although the numerical method involves a direct integration of (2.1) with the initial vorticity distribution (symmetric vortex plus dipole) described above, the Kasahara–Platzman scheme for analysing the subsequent vortex motion regards the asymmetric component as a part of the environment, even at the initial instant. In this problem, the term 'secondary flow' might seem more appropriate than 'environmental flow'. However, we shall retain the latter expression for consistency with our earlier discussion, and that which follows in part II, whilst using the terms 'asymmetric' and 'environmental' interchangeably as earlier.

Figure 11 shows the evolution of the asymmetric vorticity component and associated

[4] This is to be expected. Even in the simplest case of a symmetric vortex moving in a uniform flow on an f plane, flow asymmetries are evident, except when the uniform flow is removed *and* the vorticity maximum is chosen as the origin of the radial coordinate.

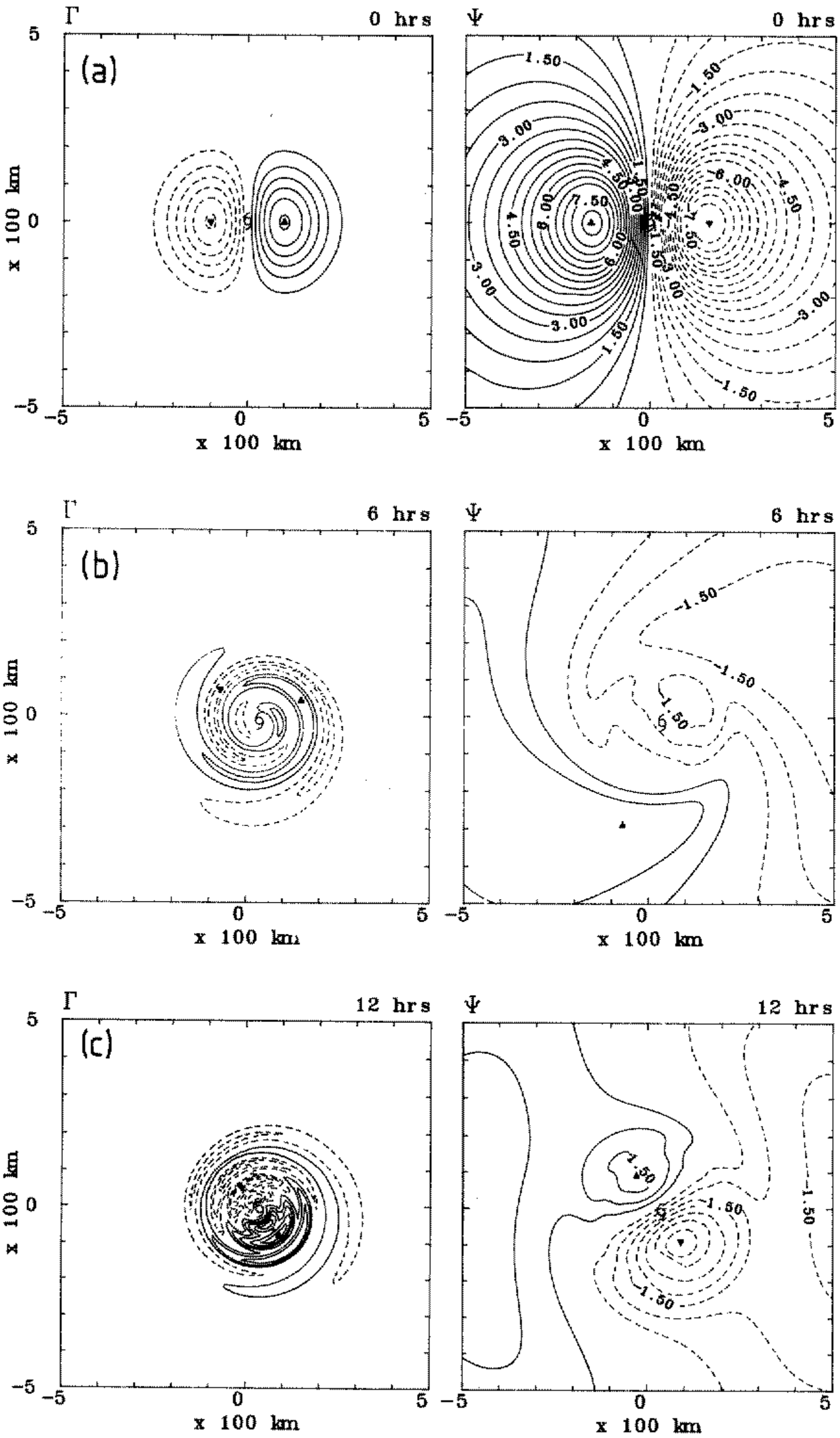

Figure 11. Evolution of the asymmetric vorticity field (Γ) and corresponding streamfunction field for the initially asymmetric vortex on an f plane in the case of small-scale asymmetry (simulation S1). Shown are (a) the initial fields, and the fields at (b) 6 hours and (c) 12 hours. Note that only one quarter of the total flow domain is shown. Contour intervals are $2\times10^{-5}s^{-1}$ for Γ and $5\times10^{4}m^{2}s^{-1}$ for Ψ. Zero contours have been excluded.

streamfunction at selected times for the calculations S1. It can be seen that within a circle of radius about $2r_{max}$ centred on the vortex, the asymmetric vorticity field undergoes rapid distortion due to the relatively large shear of the tangential wind field in this region. For example, for the flow parameters chosen, the angular velocity of the symmetric vortex decreases steadily with radius so that in 6 h an air parcel of 20 km radius completes approximately 2·4 revolutions compared with 1·4 revolutions at 100 km (i.e. r_{max}) and 0·5 revolutions at 200 km. Outside this circle, the distortion of the asymmetry proceeds more slowly. Initially, the asymmetric flow across the vortex is towards the south (Fig. 11(a)), but its direction rotates counterclockwise with the gyres of the asymmetric streamfunction as the vorticity asymmetry is rotated. Therefore the vortex track forms a counterclockwise arc as shown in Fig. 12(a). As the asymmetric vorticity distribution is wound around the vortex by the basic shear of the tangential wind, the associated flow is reduced in strength and after about 12 h, the vortex essentially stalls.

The reduction in strength of the asymmetric flow as the asymmetric vorticity field suffers angular shear can be understood in terms of an analytic solution for the problem

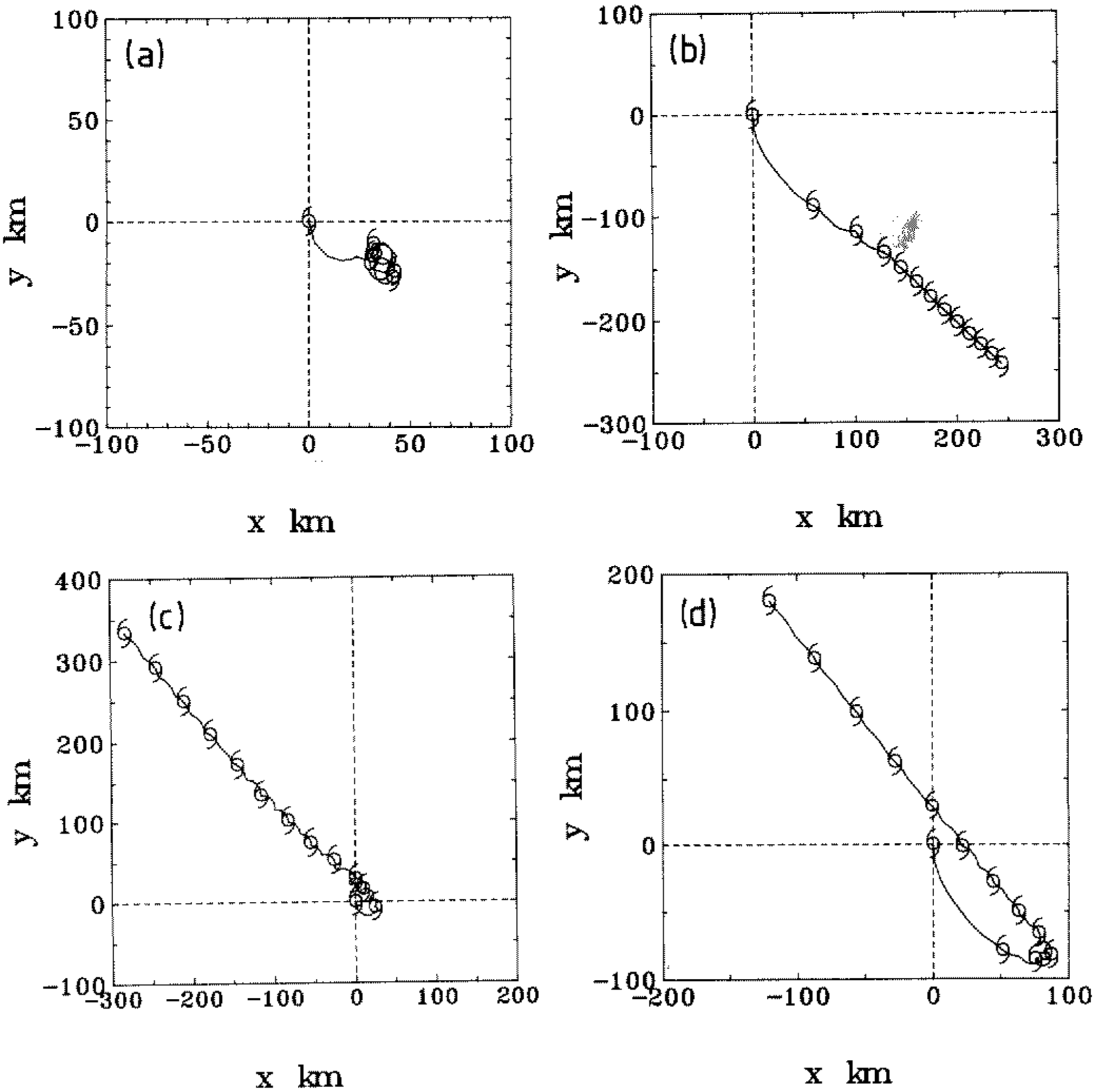

Figure 12. Tracks of initially asymmetric vortices in the calculations S1 to S4 defined in the text. (a) Small asymmetry, f plane; (b) large asymmetry, f plane; (c) small asymmetry, β plane; and (d) large asymmetry, β plane.

in which the motion of the basic vortex is ignored. Then, in the same spirit as the calculation leading to (4.2), we can show that the asymmetric vorticity distribution at time t is given by

$$\zeta_a(r,\theta,t) = \zeta_D(r/d)^2 \exp(-r^2/d^2)\cos(\theta - \Omega(r)t). \tag{5.2}$$

For an unbounded domain, we can solve the Poisson equation for the associated streamfunction using the method described by Adem (1956). Using complex notation $U_o + iV_o$, the velocity of the asymmetric flow across the vortex centre may be shown to have the form

$$U_o + iV_o = -i\zeta_D r_{max} \int_0^\infty (\eta s)^2 \exp[-\eta^2 s^2 + i(V_{max}t/r_{max})\Omega'(s)]\, ds \tag{5.3}$$

where $\eta = r_{max}/d$ and $\Omega'(s) = r_{max}\Omega(r)/V_{max}$. Further details are given in appendix B. For large values of t (i.e. $t \gg r_{max}/V_{max} = 42$ min), the integrand in (5.3) oscillates rapidly. As t increases, these oscillations become more numerous and as a result of cancellation the integral itself decreases monotonically in value.

Figure 13 shows the evolution of the asymmetric vorticity field for S2 and Fig. 12(b) shows the vortex track in this simulation. As expected, since the asymmetry is concentrated at a larger radius than S1, it is less rapidly wound up by the radial shear of the basic vortex. Accordingly, the asymmetric component of flow across the stream-

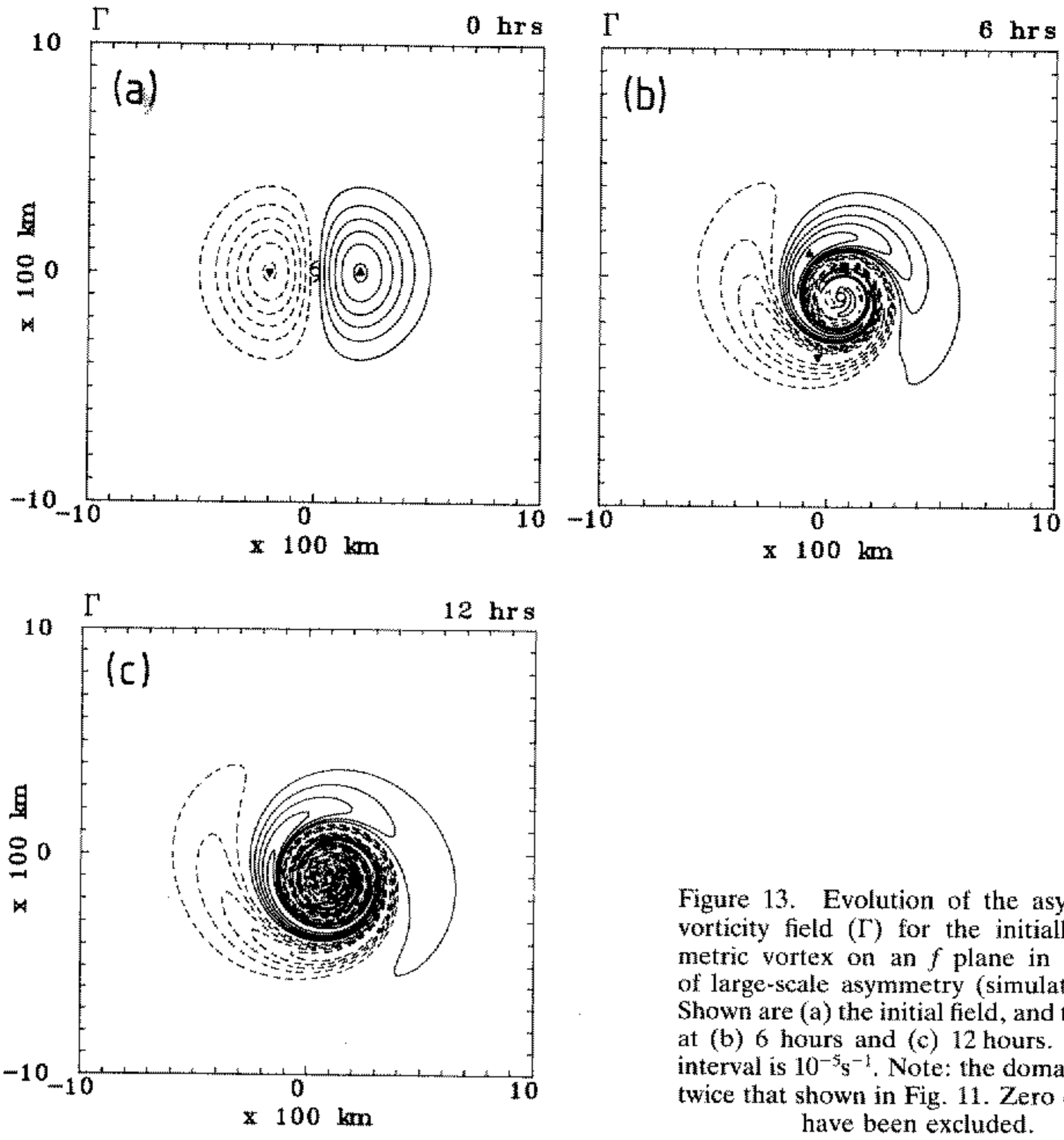

Figure 13. Evolution of the asymmetric vorticity field (Γ) for the initially asymmetric vortex on an f plane in the case of large-scale asymmetry (simulation S2). Shown are (a) the initial field, and the fields at (b) 6 hours and (c) 12 hours. Contour interval is $10^{-5}s^{-1}$. Note: the domain size is twice that shown in Fig. 11. Zero contours have been excluded.

function centre rotates less rapidly and decays less rapidly in strength. As a result, the vortex moves farther from its initial position than in S1 and its track rotates only slowly towards the east after the first three hours.

As might be anticipated from the results of section 4, the effect of a nonzero beta would be to induce an east–west vorticity tendency in addition to the existing asymmetry. This is confirmed by the calculations S3 and S4. The vortex tracks for these are shown in Figs. 12(c) and (d). In S3, the vortex no longer stalls after 12 hours, but recurves to move along a north-westwards track as the beta-induced asymmetries begin to dominate. In S4, the beta effect becomes important also, but not so rapidly, and again the track turns north-westwards as it does so.

These calculations show that the importance of vortex asymmetry on the track depends strongly on the scale of the asymmetry. The larger the scale, the less rapidly can the asymmetry be wound up by the vortex circulation and the more persistent is the effect of the asymmetry. It is evident that initial asymmetries concentrated outside the radius of maximum tangential wind can have a significant effect on subsequent vortex positions and would need to be resolved or somehow represented, even in barotropic vortex models, if predictions with a significantly improved accuracy than is at present possible are to be realized. Since routine measurement of such asymmetries are unlikely to be technically feasible for some time, it may be preferable to initialize with an asymmetric vortex designed to move with the observed speed and direction of the particular cyclone. While the design of such vortices is beyond the scope of the present work, the calculations provide a starting point for the development of such vortices and we are currently pursuing this idea.

To conclude our study of vortex asymmetry we show calculations for two interacting vortices, both initially symmetric, but of different strengths. The first calculation, designated S5, is on an f plane; the second, S6, is the beta-plane equivalent. Figure 14(a) shows the initial vorticity distribution in both cases. The stronger vortex is centred at the origin and is identical with that in section 4. The weaker vortex is centred 400 km to the east and has the same profile as the stronger, but only one fifth the strength. Figure 14(b) shows the vorticity distribution in S5 after 24 h of integration. It shows strikingly how the weaker vortex suffers rapid distortion in the tangential shear of the stronger one as it rotates around the latter. At the same time the stronger vortex centre is displaced as it moves under the influence of the streamflow associated partly with the vorticity distribution of the weaker vortex and partly with the asymmetric vorticity distribution it acquires itself from the shearing effect of the weaker vortex. If, as before, we consider departures from the vorticity field of the stronger vortex as part of its environment, and similarly for the streamfunction, the environmental streamfunction at 24 h has the structure shown in Fig. 14(c). The position of the larger vortex is denoted by the cyclone symbol and it will be seen that at this time, it is subject to a westerly flow across its centre.

The track of the stronger vortex is shown in Fig. 15(a). Initially it is towards the south, a reflection of the initial streamflow across its centre associated with the weaker vortex. Subsequently the motion vector rotates counterclockwise as the weaker vortex (and hence the circulation it induces) rotates counterclockwise around the stronger vortex. Moreover, the speed of movement reduces as the coherence of the weaker vortex is destroyed by the shearing effect of the stronger one and, as in calculation S1, the vortex ultimately stalls.

The effects of β are much as would have been anticipated from the results of calculations S3 and S4. In S5, the total vorticity distribution at 24 h[5], plotted with the

[5] For economy of space, these fields are not shown.

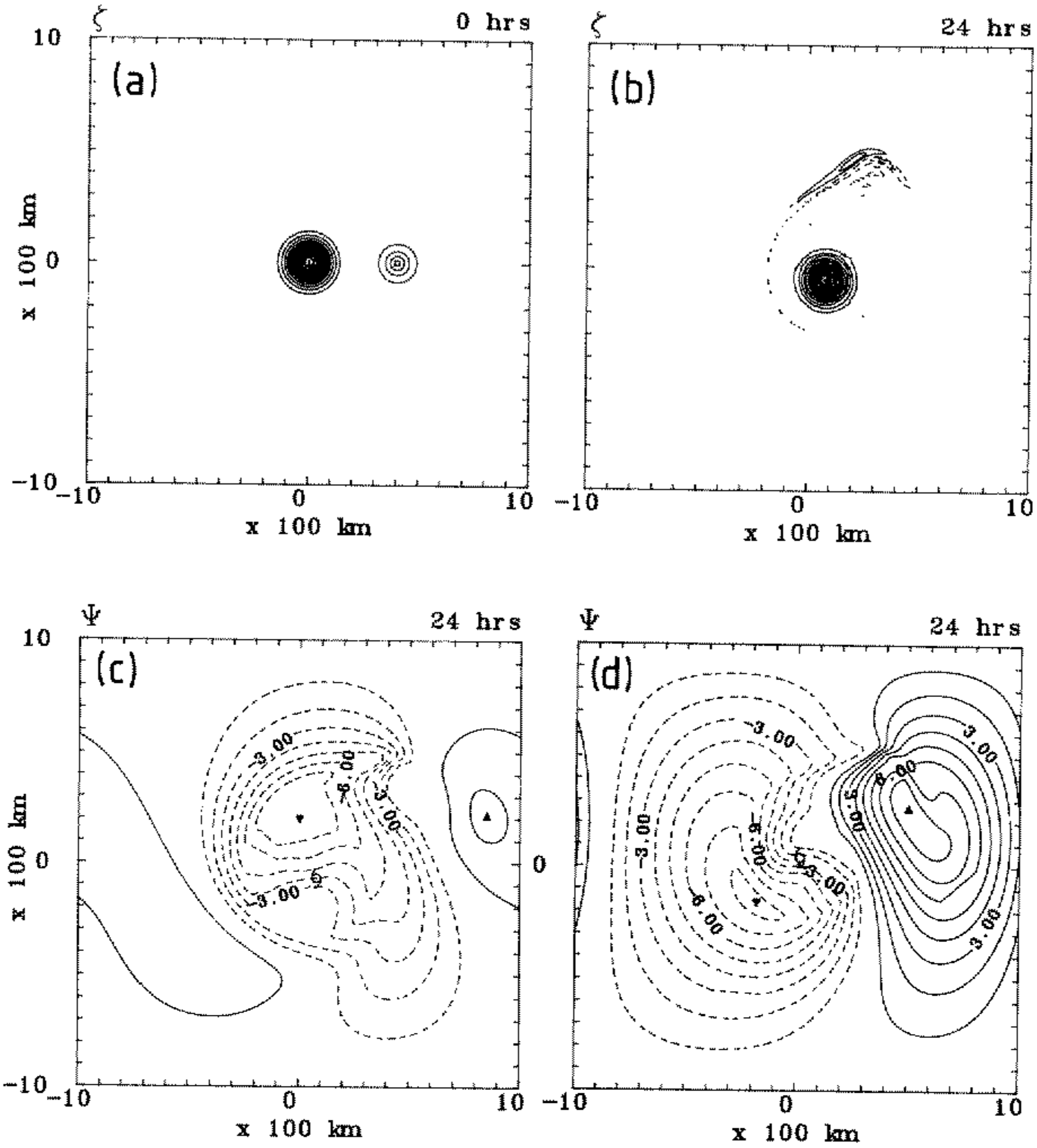

Figure 14. Total relative vorticity fields, (a) at the initial instant, and (b) at 24 hours in the case of strong-vortex, weak-vortex interaction on an f plane. The contour interval is $1{\cdot}0\times10^{-4}s^{-1}$. Shown in (c) is the corresponding environmental streamfunction field at 24 hours, 'environmental' being defined relative to the large vortex. (d) Shows the same streamfunction field for the case of the vortices interacting on a β plane. Contour intervals in (c) and (d) are $10^5m^2s^{-1}$. Zero contours have been excluded.

same contour interval as Fig. 14(b), shows only minor differences from that when $\beta = 0$, but there are noticeable differences in the asymmetric vorticity pattern resulting from the advection of planetary vorticity. These differences are reflected in the environmental streamfunction pattern shown in Fig. 14(d), where the familiar beta gyres are a dominant feature. Figure 15(b) shows the vortex track in the calculation S6. In comparison with the track of S5, the stronger vortex executes a relatively small initial loop and after only 12 h the beta effect has become dominant. After this time, the stronger vortex tracks north-westwards, but the path shows small irregularities caused by the continuing presence of the asymmetry resulting from the demise of the weaker vortex. These diminish in time, however, as the asymmetry is progressively reduced to finer scales by shear.

Further studies of the merging of two vortices as described above have been carried out by Wang and Zhu (1989) using a similar model to the present one. The results of calculations S5 and S6 are consistent with, and complement, the latter. However, Wang and Zhu investigate also the Fujiwhara effect wherein two interacting vortices of similar

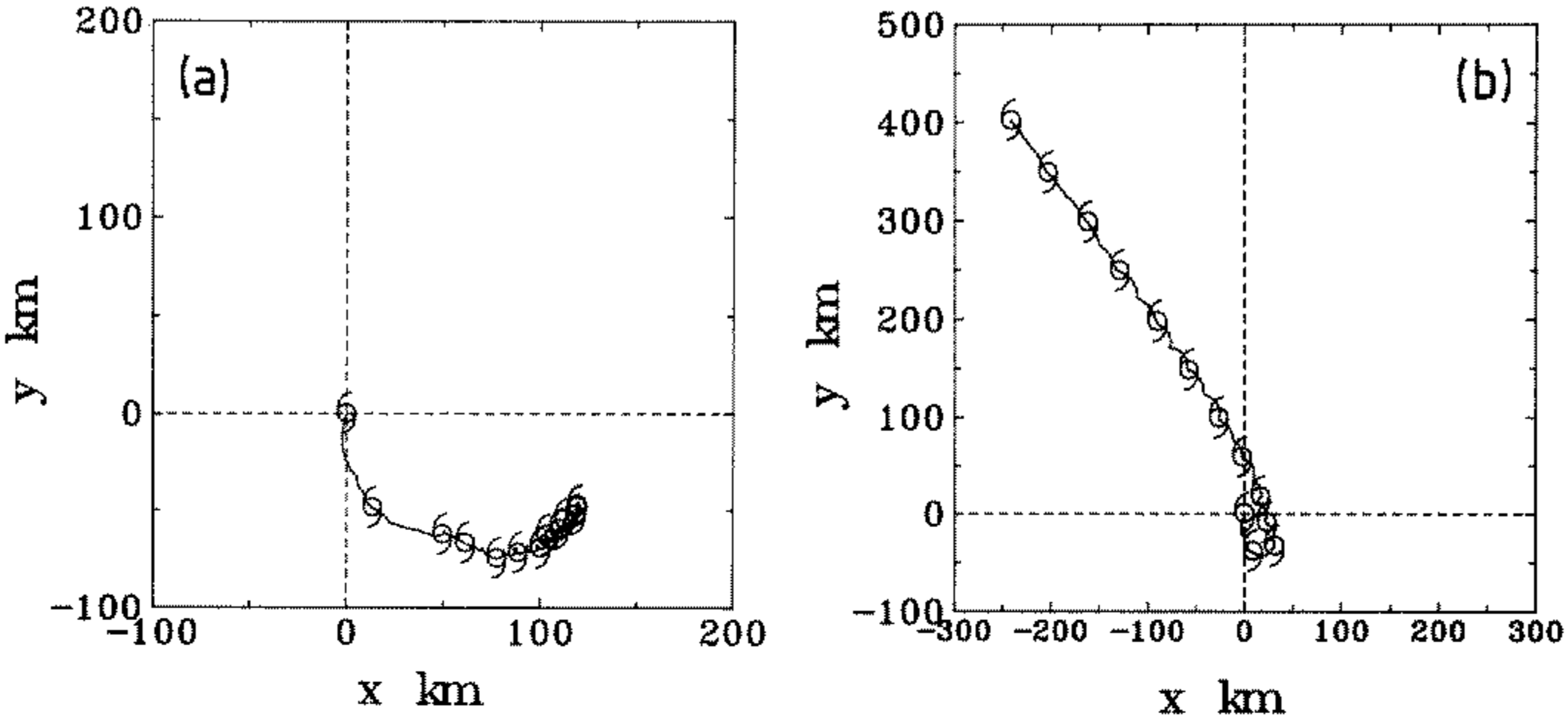

Figure 15. Tracks of the large vortex in the case of a strong-vortex, weak-vortex interaction, (a) on an f plane, and (b) on a β plane. Cyclone symbols denote successive six-hour positions, the initial position being at the origin in each case.

strength rotate around each other without merging, and they go on to explore the conditions under which a pair of vortices merge.

6. Conclusion

The role of vortex asymmetries on the motion of barotropic vortices on an f plane and on a beta plane have been explored using a nondivergent numerical model. It is shown that in the scheme for partitioning the flow between the vortex and the environment devised by Kasahara and Platzman, the environmental flow represents a steering current for the vortex. Accordingly the model provides a basis for assessing methods to extract an environmental flow from observational data on tropical cyclones. Our calculations suggest that the regions of averaging in observational studies to date are too large for this purpose.

Detailed diagnostics of the evolution of asymmetries in both the vorticity and streamfunction fields have been carried out for an initially symmetric vortex on a beta plane. These highlight the role of radial shear of the tangential wind in the inner region of the vortex in reducing the asymmetry to progressively smaller scales and emphasize the intrinsically unsteady nature of the dynamics, notwithstanding the ultimate effects of boundaries.

We have described a simple analytic model that helps to understand the evolution both of asymmetries initially present and of those that are generated as a result of the beta effect, including their scale, strength and orientation. The theory illustrates also how initial asymmetries decay in the absence of the beta effect and enables the decay rate to be quantified.

Numerical calculations for initially asymmetric vortices on a beta plane show how the scale of the asymmetry has a major influence on the subsequent vortex track, the effect being larger and more prolonged the larger the scale. The case of interaction between a strong vortex and a weaker one has been studied also. Eventually, the weaker vortex is destroyed by the tangential shear of the larger one, but in the early stages of interaction the effect on the track is appreciable. The diagnostics described provide a framework for understanding this effect.

ACKNOWLEDGMENTS

We thank Lloyd Shapiro and Greg Holland for their perceptive comments on an earlier version of the manuscript. We gratefully acknowledge support for this work from the US Office of Naval Research through grant No. N 00014-87-J-1250.

APPENDIX A

The vortex-centre-finding method

The accuracy of the diagnostics presented in this paper rely heavily on the accuracy of the numerical procedure for locating the vortex centre. We have found the scheme used by Wang and Zhu (1989) to be accurate and easy to implement. Briefly, the method is as follows. First, the grid point with the maximum vorticity is located. Then a quadratic function

$$G(x, y) = ax^2 + by^2 + cx + dy + f \tag{A1}$$

is fitted to the vorticity at this and the surrounding four points, whereupon the coefficients a, b, c, d and f can be determined. The vortex centre is taken to be the position of the maximum of this function which, relative to the position of the grid-point maximum, is $(-c/2a, -d/2b)$. At a maximum, of course, $a < 0$ and $b < 0$. The accuracy of this procedure was checked using analytic vorticity distributions with the maximum vorticity located at various positions between four grid points.

APPENDIX B

The derivation of Eq. (5.3)

Consider a vortex dipole initially with the form

$$\zeta_a(r, \theta, 0) = \zeta_D g(r) \cos\theta \tag{B1}$$

superimposed on an initially symmetric vortex characterized by the angular velocity distribution $\Omega(r)$. If the subsequent vorticity distribution can be attributed solely to advection by the symmetric vortex whose centre remains fixed, the asymmetric vorticity at time t is $\zeta_a(r, \theta, t) = \zeta_a(r, \theta - \Omega(r), 0)$. Using (B1), this may be written

$$\zeta_a(r, \theta, t) = \zeta_1(r, t) \cos\theta + \zeta_2(r, t) \sin\theta \tag{B2}$$

where, using complex notation,

$$\zeta_1 + i\zeta_2 = \zeta_D g(r) \exp[i\Omega(r)t]. \tag{B3}$$

For an infinite domain, it follows from the analysis presented by Adem (1956, see Eq. (3)) that the asymmetric streamfunction ψ_a associated with the vorticity distribution (B2) is

$$\psi_a(r, \theta, t) = \psi_1(r, t) \cos\theta + \psi_2(r, t) \sin\theta \tag{B4}$$

where

$$\psi_n(r, t) = -\frac{r}{2}\int_r^\infty \zeta_n(\sigma, t)\, d\sigma - \frac{1}{2r}\int_0^r \sigma^2 \zeta_n(\sigma, t)\, d\sigma. \tag{B5}$$

Further, for relatively mild conditions on $\zeta_n(r,t)$, e.g. ζ_n is a continuous function with a finite integral from $r=0$ to ∞, it readily follows that

$$\left.\frac{\partial \psi_n}{\partial r}\right|_{r=0} = -\frac{1}{2}\int_0^\infty \zeta_n(\sigma,t)\,d\sigma = I_n(t), \text{ say.} \tag{B6}$$

The asymmetric velocity at the origin at time t is

$$U_o(t) = \left(-\left.\frac{\partial \psi_a}{\partial y}\right|_{r=0}, \left.\frac{\partial \psi_a}{\partial x}\right|_{r=0} \right)$$

which can be evaluated by transforming the derivatives to polar form and using (B4) and (B6). It follows that $\mathbf{U}_o = (U_o, V_o)$ can be expressed in complex form by

$$U_o + iV_o = -\frac{i}{2}\int_0^\infty (\zeta_1 + i\zeta_2)\,d\sigma, \qquad = -\frac{i}{2}\zeta_D \int_0^\infty g(\sigma)\exp[i\Omega(\sigma)t]\,d\sigma. \tag{B7}$$

Equation (5.3) follows by substituting the appropriate functional forms for $g(\sigma)$ from Eq. (5.1) and $\Omega(\sigma) = V(\sigma)/\sigma$, where $V(r)$ is the tangential velocity distribution derived from Eq. (2.3).

Note that when $t = 0$

$$U_o + iV_o = -\frac{i}{2}\zeta_D d \int_0^\infty u^2 e^{-u^2}\,du \tag{B8}$$

i.e. $U_o = 0$ and V_o is proportional to $\zeta_D d$. Furthermore, for solid body rotation (Ω = constant), the asymmetry is rotated without being sheared and (B7) predicts that $U_o + iV_o$ rotates without change of magnitude, as it should.

References

Adem, J. 1956 A series solution for the barotropic vorticity equation and its application in the study of atmospheric vortices. *Tellus*, **8**, 364–372

Anthes, R. A. 1982 Tropical cyclones: their evolution, structure and effects. *Meteorological Monographs*, **19**, No. 41. American Meteorological Society

Anthes, R. A. and Hoke, J. A. 1975 The effect of horizontal divergence and the latitudinal variation of the Coriolis parameter on the drift of model hurricane. *Mon. Weather Rev.*, **103**, 757–763

Chan, J. C. L. and Gray, W. M. 1982 Tropical cyclone movement and surrounding flow relationships. *ibid.*, **110**, 1354–1374

Chan, J. C. and Williams R. T. CW1987 Analytical and numerical studies of the beta-effect in tropical cyclone motion. Part I: Zero mean flow. *J. Atmos. Sci.*, **44**, 1257–1265

DeMaria, M. 1985 Tropical cyclone motion in a nondivergent barotropic model. *Mon. Weather Rev.*, **113** 1199–1210

1987 Tropical cyclone track prediction with a barotropic spectral model. *ibid.*, **115**, 2346–2357

Fiorino, M. 1987 'The role of vortex structure in tropical cyclone motion'. Ph.D. thesis, Naval Postgraduate School, Monterey, Calif., U.S.A.

Fiorino, M. and Elsberry, R. FE 1989 Some aspects of vortex structure related to tropical cyclone motion. *J. Atmos. Sci.*, **46**, 975–990

George, J. E. and Gray, W. M. 1976 Tropical cyclone motion and surrounding parameter relationships *J. Appl. Meteorol.*, **15**, 1252–1264

Holland, G. J. 1983 Tropical cyclone motion: environmental interaction plus a beta-effect. *J. Atmos. Sci.*, **40**, 328–342

Hoskins, B. J., McIntyre, M. E. and Robertson, A. W. 1985 On the use of isentropic potential vorticity maps. *Q. J. R. Meteorol. Soc.*, **111**, 877–946

Kasahara A.	1957	The numerical prediction of hurricane movement with the barotropic model. *J. Meteorol.*, **14,** 386–402
	1960	The numerical prediction of hurricane movement with a two-level baroclinic model. *ibid.*, **17,** 357–370
Kasahara, A. and Platzman, G. W.	1963	Interaction of a hurricane with a steering field and its effect upon the hurricane trajectory. *Tellus*, **15,** 321–335
Kitade, T.	1980	Numerical experiments of tropical cyclones on a plane with variable Coriolis parameter. *J. Meteorol. Soc. Jap.*, **58,** 471–488
Sanders, F.	1970	Dynamic forecasting of tropical storm tracks. *Trans. New York Acad. Sci.*, **32,** 495–508
Sanders, F. and Burpee R. W.	1968	Experiments in barotropic hurricane track forecasting. *J. Appl. Meteorol.*, **7,** 313–323
Sanders, F., Pike, A. C. and Gaertner, J. P.	1975	A barotropic model for operational prediction of tracks of tropical storms. *ibid.*, **14,** 265–280
Sanders, F., Adams, A. L., Gordon, N. J. B. and Jensen, W. D.	1980	Further development of a barotropic operational model for predicting paths of tropical storms. *Mon. Weather Rev.*, **108,** 642–654
Sasaki, Y.	1955	Barotropic forecasting for the displacement of a typhoon. *J. Meteorol. Soc. Jap.*, **33,** 1–8
Sasaki, Y. and Miyakoda, K.	1954	Numerical forecasting of the movement of cyclone. *ibid.*, **32,** 9–19
Sutcliffe, R. C.	1947	A contribution to the problem of development. *Q. J. R. Meteorol. Soc.*, **73,** 370–383
Wang, Y. and Zhu, Y.	1989	A numerical study on the Fujiwhara effect of two interacting cyclonic vortices. *J. Acad. Meteorol. Sci., SMA, China*, **4,** 13–19 (in Chinese)